Solid State Ionics 368 (2021) 115699

Contents lists available at ScienceDirect

Solid State Ionics

journal homepage: www.elsevier.com/locate/ssi

Reaction kinetics in the system Y_2O_3/Al_2O_3 – A solid state reaction forming multiple product phases investigated by using thin film techniques

Carsten Korte [a,*], Bernhard Franz [b]

[a] Institut für Energie und Klimaforschung (IEK-14: Elektrochemische Verfahrenstechnik), Forschungszentrum Jülich, 52425 Jülich, Germany
[b] Physikalisch-Chemisches Institut, Justus-Liebig Universiät Gießen, Heinrich-Buff-Ring 58, 35392 Gießen, Germany

ARTICLE INFO

Keywords:
Heterogeneous solid state reactions
Al_2O_3–Y_2O_3 multiple product phases
YAG–YAP–YAM
Coupled growth kinetics
Parabolic rate constants

ABSTRACT

The kinetics of the heterogeneous solid state reaction between Al_2O_3 and Y_2O_3 is investigated by using thin film techniques. Y_2O_3 films are grown by means of pulsed laser deposition (PLD) on single crystalline alumina substrates with a (0001) orientation. The solid state reactions are performed at a temperature of 1400 °C (1673 K). The cross sections of the reacted samples were investigated by means of SEM and XRD and exhibit a sequence of three product layers, $Y_3Al_5O_{12}$ (YAG), $YAlO_3$ (YAP) and $Y_4Al_2O_9$ (YAM). The simultaneous growth of the product layers is controlled by a diffusional kinetics and the thickness increases are coupled to each other. According to Wagner and Schmalzried, one has to distinguish between rate constants of the first kind ("practical" Tammann constant), in the case of simultanous and coupled growth of multiple product phases, and rate constants of the second kind ("true" Tammann constant), in the case of the uncoupled and only growth of one product phase in equilibrium with the adjacent phases. The growth kinetics for a solid reaction forming three product phases (layer) is analysed in detail using linear transport theory. For the formation of YAG, YAP and YAM the rate constants of the second kind are determined from the experimental data and those of the first kind are calculated and compared to the available literature data. Based on these considerations, a detailed overview about the phase formation kinetics in the temperature range of 1200–1400 °C can be given for the first time. The (Nernst-Planck coupled) cation conductivities are calculated.

1. Introduction

Solid state reactions play an important role in high temperature corrosion processes. The formation of a degradation layer covering a device, due to the reaction with ambient air or the formation of an interphase layer between two solid components, can be treated as a diffusion-controlled heterogeneous reaction. The synthesis of functional ceramics by sintering of powderous educts is also controlled by analogue processes at the contact points of the adjoined particles.

Considering oxide materials, the prerequisite for a diffusion-controlled heterogeneous solid state reaction is the mobility of cations and/or oxide anions. If only one ternary compound exists in the quasi-binary phase field of two binary starting oxides, the reaction product is formed as a single continous layer between the starting materials. The growth kinetics of the diffusion-controlled product layer formation depend on the thickness of the product layer. It can be fully characterised by a single parabolic (Tammann) rate constant and its activation energy. [1,2]

If more than one ternary compound exists in the phase field of the two binary oxides, the diffusion-controlled sequence of reactions is much more complex. A sequence of more than one product layer can in principial be formed. The growth kinetics of a distinct product layer are coupled to those of the adjacent layers. According to Wagner and Schmalzried, it is necessary to distinguish between rate constants of the first kind ("practical" rate constants) when the sequence of product layers is simultaneously formed in a reaction and rate constants of the second kind ("true" rate constants) when considering the insulated and uncoupled growth of a single product layer. [1–3]

Many oxide materials of technological importance, such as garnets or perovskites are formed as a product in a multi-product solid state reaction. In the case of a (kinetically-formed) sequence of (intermediate) products, the finally obtained product(s) depend in a delicate way on the reaction time and on the stoichoimetry of the starting materials. [4] To apply new preparation methods, but also to understand degradation processes in thin film systems, it is important to know the reaction kinetics of these product formation sequences.

---

* Corresponding author.
E-mail address: c.korte@fz-juelich.de (C. Korte).

https://doi.org/10.1016/j.ssi.2021.115699
Received 29 April 2021; Received in revised form 10 June 2021; Accepted 18 June 2021

In the case of the Al_2O_3–Y_2O_3 system, many experimental studies have been performed to elucidate the product phase formation as a function of temperature and the molar ratio of the starting oxides. [4–8] The product phases $Y_3Al_5O_{12}$ (YAG) and $YAlO_3$ (YAP) are used as host material for rare-earth metal cations for applications as phoshors, luminophors or solid-state laser materials. Ca-doped YAP is discussed as an electrolyte for solid oxide fule cells (SOFC). [9] In theses studies the reaction between powdery educts is investigated using diffraction methods, kinetic data in the sense of parabolic rate constants is not available. Experimental studies on such multinary reaction sequences performed on geometrically-defined thin film samples is fairly sparse. [10–12] The latter is a prerequisite for conducting precise measurements to obtain these data. Thus, in this study we focus on thin film experiments on the Al_2O_3–Y_2O_3 system and a detailed formal analysis.

2. Formal considerations

2.1. Heterogeneous solid state reactions with multiple product phases

If several ternary compounds exist in the quasi-binary phase field of two binary oxides, they can principially be formed as products in a (diffusion-limited) heterogeneous solid state reaction. The product phases will appear in a sequence of layers embedded between the the starting oxides, controlled by the activity gradients of the reactants [1–3]. As a model for a heterogeneus solid state reaction forming multiple product phases the reaction between two trivalent oxides A_2O_3 and B_2O_3, forming a 3:5 product $A_3B_5O_{12}$, a 1:1 product ABO_3 and a 2:1 product $A_4B_2O_9$ is treated exemplarily. This is a typical sequence that can be observed for the reaction of Al_2O_3 and rare earth sesquioxides RE_2O_3:

Al_2O_3 – Y_2O_3 [4,6–8,10], see also Fig. 2.
→ $Y_3Al_5O_{12}$ (YAG), $YAlO_3$ (YAP), $Y_4Al_2O_9$ (YAM)
Al_2O_3 – Gd_2O_3 [4,13,14]
→ $GdAlO_3$ (GAP), $Gd_4Al_2O_9$ (GAM)
Al_2O_3 – Yb_2O_3 [4]
→ $Yb_3Al_5O_{12}$ (YbAG), $Yb_4Al_2O_9$ (YbAM)

For the further treatment, the two trivalent oxides will be denoted by A_2O_3 and B_2O_3. A^{3+} and B^{3+} are general trivalent cations. In the case of the rare earth sesquioxides RE_2O_3, the 3:5 product $A_3B_5O_{12}$ usually has a cubic garnet structure, the 1:1 product ABO_3 has a (orthorhombic distorted) perovskite structure and the 2:1 product $A_4B_2O_9$ a monoclinic cuspidine structure. For the sake of brevity, all quantities that are related to one of the product phases $A_4B_2O_9$, ABO_3 or $A_3B_5O_{12}$ will be marked with a capital letter according to their structure (M: monoclinic phase, P: perovskite and G: garnet). If all three products are formed from the starting oxides A_2O_3 and B_2O_3, the following reactions will take place in the layer sequence between the neighbouring phases:

$$\mathrm{M}: \mathrm{A_2O_3} + 2\mathrm{ABO_3} = \mathrm{A_4B_2O_9} \quad (1)$$

$$\mathrm{P}: \mathrm{A_4B_2O_9} + \mathrm{A_3B_5O_{12}} = 7\mathrm{ABO_3} \quad (2)$$

$$\mathrm{G}: 3\mathrm{ABO_3} + \mathrm{B_2O_3} = \mathrm{A_3B_5O_{12}} \quad (3)$$

In the following, we will assume a simple planar geometry between the starting oxides and product layers, as depicted in Fig. 1. The cations A^{2+} and B^{3+} have a sufficent mobility in the product phases. Fluxes of O^{2-} anions and of electronic charge carriers are neglected in the further treatment for the sake of simplicity (see also Appendix A). There is no access of oxygen from the surrounding atmosphere to the phase boundaries B_2O_3/G, G/P, P/M and M/A_2O_3. The total reactions in Eq. (1), (2) and (3) can be diveded up in partial reactions for each phase boundary:

$$\mathrm{M/A_2O_3}: \mathrm{A_4B_2O_9} + 2\mathrm{A^{3+}} = 3\mathrm{A_2O_3} + 2\mathrm{B^{3+}} \quad (4)$$

$$\mathrm{P/M}: 3\mathrm{ABO_3} + \mathrm{A^{3+}} = \mathrm{A_4B_2O_9} + \mathrm{B^{3+}} \quad (5)$$

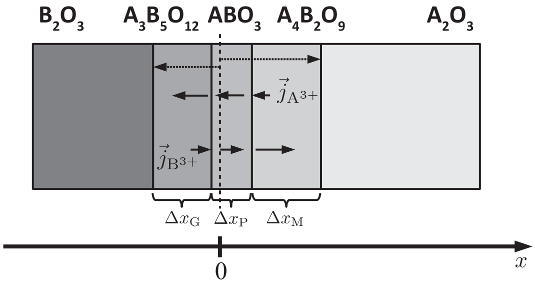

Fig. 1. Simultaneous and coupled growth of the three product phases (layers) from the two starting oxides (sesquioxides). The cation fluxes $\vec{j}_{A^{3+}}$ and $\vec{j}_{B^{3+}}$ in the layer sequence are indicated by arrows. The initial interface between the starting oxides is marked with a dashed line at $x = 0$.

$$\mathrm{G/P}: \mathrm{A_3B_5O_{12}} + \mathrm{A^{3+}} = 4\mathrm{ABO_3} + \mathrm{B^{3+}} \quad (6)$$

$$\mathrm{B_2O_3/G}: 4\mathrm{B_2O_3} + 3\mathrm{A^{3+}} = \mathrm{A_3B_5O_{12}} + 3\mathrm{B^{3+}} \quad (7)$$

Eq. (4) to (7) are written in a form that the progressing reaction will move the phase boundaries in Fig. (1) to the left. In the case of the reaction system $Al_2O_3 - Y_2O_3$ (A = Al and B = Y), as depicted in Fig. 2, the partial reactions in Eq. (4) to (7) are indicated in the quasi-binary phase diagram with the equation numbers (in parentheses). We assume that no redox reactions will take place at the phase boundaries, which could lead to the formation of pores or to the precipitation of metal.

2.2. Description by linear transport theory

The fluxes of the cations in the product layers are coupled due to the condition of electroneutrality. With regard to the stoichiometry of the boundary reaction driving the reaction fronts, the simultanous and coupled formation of the product layers can be described in terms of linear transport theory. The general description is given by Wagner and Schmalzried. [1–3] A solid state reaction forming two product phases is treated by Borchard et al. [17] The treatment for a solid state reaction forming three product phases as described in Eq. (4) to (7) is provided in

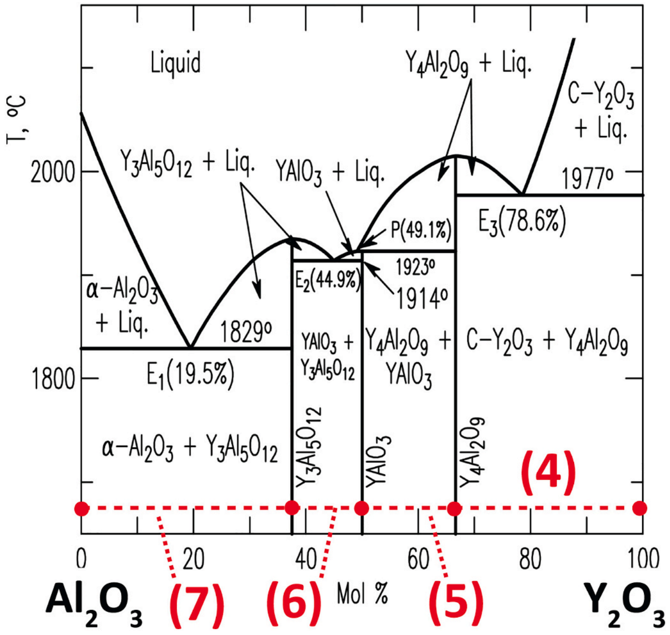

Fig. 2. Phase diagram of the (pseudo-) binary system Al_2O_3 – Y_2O_3 according”Phase Diagrams for Ceramists“, American Ceramic Society. [15,16] The numbers in brackets correspond to the reactions given in Eq. (4) to (7).

Appendix A.

Assuming the independent growth of the product layers, *e.g.* when providing $A_4B_2O_9$ and $A_3B_5O_{12}$ as starting materials to grow the ABO_3 phase, the "true" uncoupled growth kinetics can be measured. Using these "true" parabolic rate constants $k_{\mathrm{Tam,\ G}}$, $k_{\mathrm{Tam,\ P}}$ and $k_{\mathrm{Tam,\ G}}$ for the uncoupled growth of the product layers and the stoichiometric factors of the interface reactions in Eq. (1) to (6), a non-linear system of ordinary differential equations (ODE) with constant coefficients can be derived, describing the simultanous and coupled growth of all product layers:

$$\frac{1}{V_{\mathrm{m}}^{\mathrm{M}}}\frac{d(\Delta x_{\mathrm{M}})}{dt}=\frac{k_{\mathrm{M}}}{V_{\mathrm{m}}^{\mathrm{M}}}\frac{1}{\Delta x_{\mathrm{M}}}-\frac{1}{7}\frac{k_{\mathrm{P}}}{V_{\mathrm{m}}^{\mathrm{P}}}\frac{1}{\Delta x_{\mathrm{P}}} \tag{8}$$

$$\frac{1}{V_{\mathrm{m}}^{\mathrm{P}}}\frac{d(\Delta x_{\mathrm{P}})}{dt}=-2\frac{k_{\mathrm{M}}}{V_{\mathrm{m}}^{\mathrm{M}}}\frac{1}{\Delta x_{\mathrm{M}}}+\frac{k_{\mathrm{P}}}{V_{\mathrm{m}}^{\mathrm{P}}}\frac{1}{\Delta x_{\mathrm{P}}}-3\frac{k_{\mathrm{G}}}{V_{\mathrm{m}}^{\mathrm{G}}}\frac{1}{\Delta x_{\mathrm{G}}} \tag{9}$$

$$\frac{1}{V_{\mathrm{m}}^{\mathrm{G}}}\frac{d(\Delta x_{\mathrm{G}})}{dt}=-\frac{1}{7}\frac{k_{\mathrm{P}}}{V_{\mathrm{m}}^{\mathrm{P}}}\frac{1}{\Delta x_{\mathrm{P}}}+\frac{k_{\mathrm{G}}}{V_{\mathrm{m}}^{\mathrm{G}}}\frac{1}{\Delta x_{\mathrm{G}}} \tag{10}$$

Hereby, Δx_{M}, Δx_{P} and Δx_{G} denote the product layer thicknesses and $V_{\mathrm{m}}^{\mathrm{M}}$, $V_{\mathrm{m}}^{\mathrm{P}}$ and $V_{\mathrm{m}}^{\mathrm{G}}$ the molar volumes.

The chemical potentials of the starting oxides A_2O_3 und B_2O_3 in each growing product layer are fixed at the interfaces by the chemical equilibria with the neighbouring product phases, see Eq. (1) to (3). Thus, simple parabolic rate laws $d(\Delta x_i)/dt = k_i'/\Delta x_i$ (i = M, P and G) should also be valid for the growth of each product layer in the case of simultaneous and coupled growth, as expected for a diffusion-limited process. [1,17] When introducing "practical" parabolic rate constants $k_{\mathrm{Tam,\ M}}'$, $k_{\mathrm{Tam,P}}'$ und $k_{\mathrm{Tam,\ G}}'$ for a solid state reaction forming multiple product phases, it yields parabolic growth laws for each product layer:

$$\Delta x_{\mathrm{M}}=\sqrt{2k_{\mathrm{Tam,M}}'\Delta t} \tag{11}$$

$$\Delta x_{\mathrm{P}}=\sqrt{2k_{\mathrm{Tam,P}}'\Delta t} \tag{12}$$

$$\Delta x_{\mathrm{G}}=\sqrt{2k_{\mathrm{Tam,G}}'\Delta t} \tag{13}$$

The approach in Eq. (11) to (13) is a general analytical solution for the system of differential equations in Eq. (8) to (10). The values of the "practical" parabolic rate constants are always smaller compared to the "true" parabolic rate constants of the independent and uncoupled formation of a single product layer. In the case of the simultanous and coupled growth of multiple product layers, a distinct product layer is at the same time the starting material for the neighbouring layers.

Using the approach in Eq. (11) to (13) to solve the system of differential equations in Eq. (8) to (10), the following relations can be derived between the "true" and "practical" parabolic rate constants:

$$\frac{k_{\mathrm{M}}}{V_{\mathrm{m}}^{\mathrm{M}}}=2\frac{k_{\mathrm{M}}'}{V_{\mathrm{m}}^{\mathrm{M}}}+\frac{1}{2}\frac{\sqrt{k_{\mathrm{M}}'k_{\mathrm{P}}'}}{V_{\mathrm{m}}^{\mathrm{P}}}+\frac{3}{2}\frac{\sqrt{k_{\mathrm{M}}'k_{\mathrm{G}}'}}{V_{\mathrm{m}}^{\mathrm{G}}} \tag{14}$$

$$\frac{k_{\mathrm{P}}}{V_{\mathrm{m}}^{\mathrm{P}}}=7\frac{\sqrt{k_{\mathrm{M}}'k_{\mathrm{P}}'}}{V_{\mathrm{m}}^{\mathrm{M}}}+\frac{7}{2}\frac{k_{\mathrm{P}}'}{V_{\mathrm{m}}^{\mathrm{P}}}+\frac{21}{2}\frac{\sqrt{k_{\mathrm{P}}'k_{\mathrm{G}}'}}{V_{\mathrm{m}}^{\mathrm{G}}} \tag{15}$$

$$\frac{k_{\mathrm{G}}}{V_{\mathrm{m}}^{\mathrm{G}}}=\frac{\sqrt{k_{\mathrm{M}}'k_{\mathrm{G}}'}}{V_{\mathrm{m}}^{\mathrm{M}}}+\frac{1}{2}\frac{\sqrt{k_{\mathrm{P}}'k_{\mathrm{G}}'}}{V_{\mathrm{m}}^{\mathrm{P}}}+\frac{5}{2}\frac{k_{\mathrm{G}}'}{V_{\mathrm{m}}^{\mathrm{G}}} \tag{16}$$

The ratio of the product layer thicknesses Δx_{M}, Δx_{P} and Δx_{G} during the growth process can be derived from Eq. (11) to (13). It depends only on the "practical" parabolic rate constants:

$$\Delta x_{\mathrm{M}}:\Delta x_{\mathrm{P}}:\Delta x_{\mathrm{G}}=\sqrt{k_{\mathrm{M}}'}:\sqrt{k_{\mathrm{P}}'}:\sqrt{k_{\mathrm{G}}'} \tag{17}$$

3. Experimental

3.1. Preparation of the thin film samples

The solid-state reaction between Al_2O_3 and Y_2O_3 has been selected as a model system that kinetically forms a sequence of three product phases. The reaction products are $Y_3Al_5O_{12}$ (YAG), $YAlO_3$ (YAP) and $Y_4Al_2O_9$ (YAM), see Fig. 2. [4,6,15]

The setup for all experiments was prepared using thin-film technology. Epi-polished Al_2O_3 single-crystal wafers with the orientation (0001) were used (CrysTec GmbH/Berlin, 10 × 10 × 0.5 mm). The Al_2O_3 substrates were coated with a Y_2O_3 layer using pulsed laser deposition (PLD). The Y_2O_3 targets were prepared by uniaxial cold pressing of Y_2O_3 powder (99.999%, Chempur/Karlsruhe) with a pressure of 60 MPa and subsequent sintering for 48 h at 1500 °C (1773 K) in air. The substrate temperature during the deposition was adjusted to 700–900 °C. Oxygen was used as a background gas in order to avoid a non-stoichiometry of the thin film oxide. The pressure was adjusted to 9 Pa ($9 \cdot 10^{-2}$ mbar). A growth rate of 1–2 μm h^{-1} could be reached at a repetition rate of 10 Hz and pulse energy of 200–250 mJ (fluence in focus 20–25 J cm^{-2}). Y_2O_3 layers with a thickness of 6–10 μm were prepared.

Depending on the results from the XRD characterisation the Y_2O_3-coated Al_2O_3 substrates were post-treated in air at 800–1000 °C for 24 h in order to increase the crystallinity. The substrates were then sawn into samples of about 4 × 2 × 0.5 mm in size.

3.2. Solid state reaction

The samples were placed in a sample holder, made of a Al_2O_3 oxide ceramic tube and covered with a platinum foil to prevent the sample surface from possible dust particles in the furnace, see Fig. 3. Initially, preliminary experiments were carried out at different temperatures and a fixed reaction time of 30 min. in order to identify a suitable reaction temperature for the subsequent time-dependent experiments. According to the results, a fixed temperature of 1400 °C was chosen. The samples were brought to the desired reaction temperature in about 60 min. (20 °C/min. until 1000 °C and 30 °C/min. from 1000 to 1400 °C) by moving the sample holder into a tubular oven at the reaction temperature and cooled down to room temperature by moving out. During the heating and cooling process the total time the samples reside in the temperature range between 1250 and 1400 °C is less than 20 min. In this temperature interval the practical parabolic rate constants will drop by two orders of magnitude according to the results by Heffelfinger et al. (see discussion). [10] Thus the resulting experimental errors may be neglectable. For the time-dependent experiments, time periods of between 1.5 and 72 h were choosen.

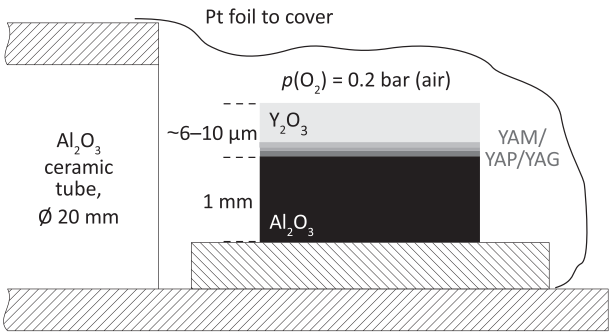

Fig. 3. Sketch of the experimental setup (not true to scale). The height of the Al_2O_3/Y_2O_3 sample is oversized. The Pt foil was used as protection against possible dust partices in the furnace and was not in contact with the sample.

3.3. Microstructural characterisation by XRD and SEM

The crystallinity, texture and orientation relationships of the crystallites in the unreacted and reacted samples were characterised by means of X-ray diffractometry (Siemens D500, Cu-K$_\alpha$, Graphite diffracted beam monochromator, Bragg-Brentano geometry).

The morphological development and the microscopic structure of the phase boundaries were characterised by using scanning electron microscopy (SEM, LEO Gemini 982). Cross sections of the reacted samples were prepared by means of mechanical polishing. The final polishing step was carried out using colloidal silicon oxide (0.01 μm). The SEM images were taken in backscattered electron mode (BSE) at 10 kV acceleration voltage in order to achieve an optimal contrast between the individual phases Al_2O_3, YAG, YAP, YAM and Y_2O_3.

4. Results

4.1. Structural chracterisation of the Y_2O_3 thin film

Y_2O_3 can be grown on Al_2O_3 substrates by PLD as a dense and contINOUS thin film up to a thickness of 10 μm. Using SEM no voids could be detected in the Y_2O_3 phase, see Fig. 4.

The as-deposited thin films have poor crystallinity. According to the results from the XRD characterisations, an FWHM of ~0.8° can be found. After the thermal treatment at 800–1000 °C, the FMWH was reduced to ~0.5°, see Fig. 5.

In addition to the very strong (0001) peak of the Al_2O_3 substrate, essentially only the (222) and (440) peak of Y_2O_3 exhibit an increased intensity compared to a (untextured) powder sample. At very low film thicknesses only the (222) peak can be detected. The intensity of the (222) peak decreases with increasing film thickness and the intensity of the (440) peak is increasing, finally exceeding the (222) peak. In an untextured powder sample, the (222) peak has a higher intensity than the (440) peak. Thus, the crystallites of a Y_2O_3 thin film growing on a (0001) Al_2O_3 surface initially have a (111) orientation. With increasing film thickness the subsequently formed crystallites prefer the (110) orientation.

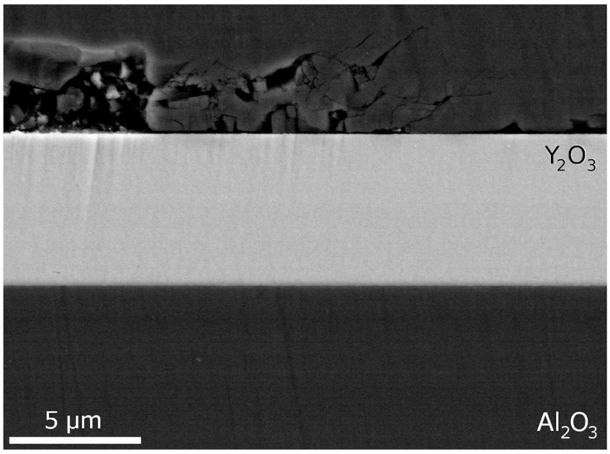

Fig. 4. Cross section of an unreacted Y_2O_3 thin film on a (0001) Al_2O_3 substrate. The images was taken in the BSE mode at an acceleration voltage of 10 kV. As Y_2O_3 has the highest average atomic mass, it appears as a bright belt on the Al_2O_3 substrate.

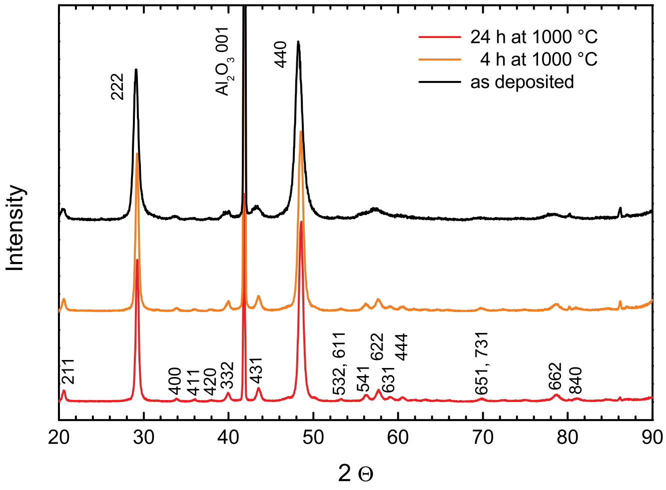

Fig. 5. Diffractogram of a Y_2O_3 thin film on a (0001) Al_2O_3 substrate with a thickness of 5.5 μm as deposited by PLD and after a heat-treatment in air at 1000 °C for 4 h and 24 h.

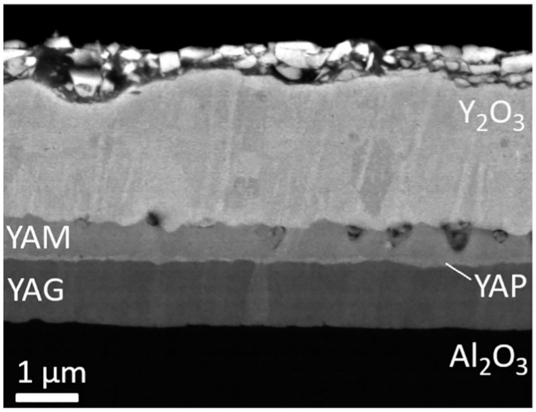

Fig. 6. SEM microslide (cross section) taken in the BSE mode of a sample after a reaction time of 15 h. The grain boundary structure in the Y_2O_3, YAG, YAP and YAM layers is partially visible due to the channeling contrast. The reaction temperature T was adjusted to 1400 °C. An acceleration voltage of 10 kV was used.

4.2. Morphology of the product layers

In order to analyse the moving phase boundaries, the cross sections of the samples are characterised by SEM. This showed that the interfaces between Y_2O_3 and the YAM product layer, respectively between the Al_2O_3 substrate and the YAG product layer were comperatively flat, see Fig. 6. The observed wavyness, respectively the triangular-like features in the interface were usually connected to grain boundaries in the adjacent phases that were partially visible in BSE imaging mode due to the channeling contrast.

In the case of the YAP phase, a uniform layer thickness was only present at very short reaction times. When the reaction proceeds, significant thickness variations appear, as shown Fig. 7. After 24 h, the size of the YAP crystallites varies in the range of 200 nm and 1.2 μm perpendicular to the moving interfaces. After 72 h, thickness variations of between 0.18 μm and 1.47 μm can be measured. Within the investigated reaction time, up to 72 h and as long as unreacted Y_2O_3 is available, the YAP phase is always the thinnest product layer.

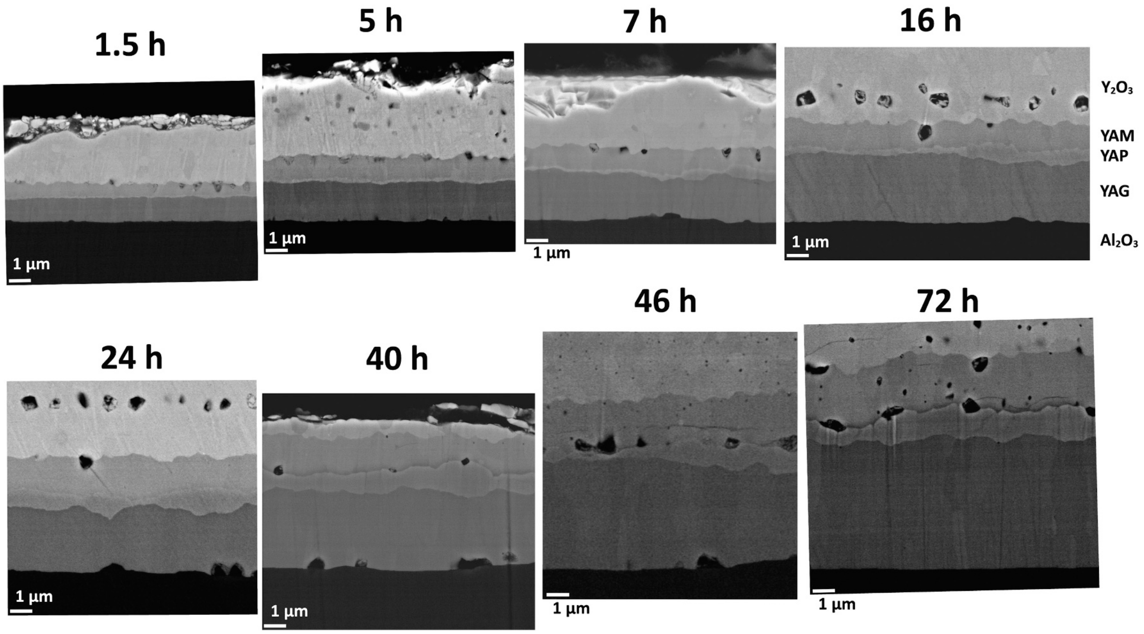

Fig. 7. SEM microslides (cross sections) taken in the BSE mode of different samples after a reaction time of 1.5 h, 5 h, 7 h, 16 h, 24 h, 40 h 46 h and 72 h. The reaction temperature T was adjusted to 1400 °C. An acceleration voltage of 10 kV was used.

A formation of pores could be observed in the Y_2O_3/YAM interface within the investigated reaction time. To a smaller extend, this is also noticable for the YAM/YAP interface. Furthermore, some samples show a noticable accumulation of pores in the remaining Y_2O_3 thin film, arranged in a line parallel to the Y_2O_3/YAM interface. The distance from the interface depends on reaction time and initial Y_2O_3 film thickness.

4.3. *Growth kinetics*

The average product layer thicknesses Δx_i (i = M, P and G) were evaluated from the SEM microslides by using the software ImageJ. [18] The errors were estimated acoording to the observed variations when performing the image analysis at different locations, respectively to the observed thickness variations. In Fig. 8, the average product layer thicknesses Δx_i (i = M, P and G) are plotted *vs.* the reaction time Δt with a double logarithmic scaling.

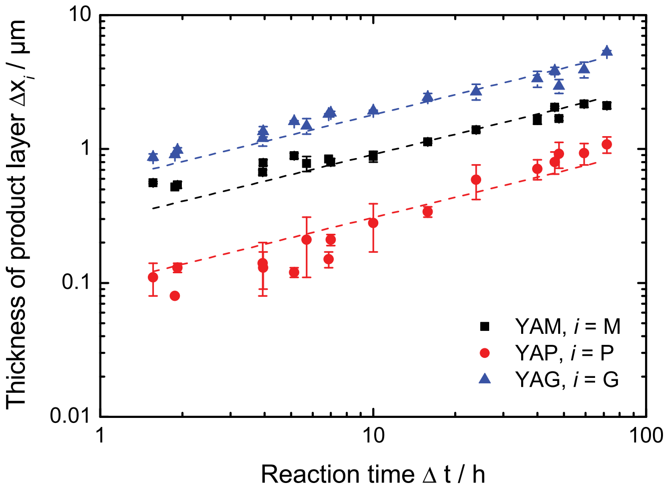

Fig. 8. Thickness Δx_i (i = M, P and G) of the product layers YAG, YAP and YAM measured by image analysis of the SEM microslides *vs.* the reaction time Δt. The reaction temperature T was adjusted to 1400 °C. The dashed lines are obtained by non-linear fitting of the tamman growth laws according Eq. (11) to (13).

5. Discussion

5.1. *Orientation of the deposited Y_2O_3 layers*

Y_2O_3 has a cubic bixbyite structure ($Ia\bar{3}$) and the Al_2O_3 substrate a trigonal corundum structure ($R\bar{3}c$). The (111) lattice planes of the Y_2O_3 thin film and the (0001) lattice planes of the Al_2O_3 substrate feature a trifold symmetry axis. This match may explain the preferential nucleation and growth of Y_2O_3 crystallites in (111) orientation on a (0001) Al_2O_3 substrate. This preferential orientation on (0001) Al_2O_3 substrates has been frequently reported in the literature. Using PLD as a deposition technique, this was observed for thin Y_2O_3 film (100 nm) by Heffelfinger et al., Johnson et al. and in own studies on Y_2O_3/YSZ multilayers. [10,11,19,20] When using spin-coating, it was also found by Arakawa et al. after a heat-treatment of the (gel-like) precursor film at 1000 °C. [12]

With increasing film thickness crystallites with other orientations will also nucleate. The XRD results suggest, that the Y_2O_3 crystallites with a (110) orientation grow faster than the others and ultimately dominate the texture in the case of thick films. This may explain the change in the preferential orientation observed by XRD.

5.2. *Morphology of the product layers*

As the observed wavyness of the Y_2O_3/YAM and Al_2O_3/YAG interface, respectively the triangular-like features are usually connected to grain boundaries in the adjacent phases, these features are most likely caused by the enhanced mass transport along these boundaries and by a preferential nucleation at the end of the boundaries, see Fig. 6. [21] This is often observed for heterogeneous solid state reactions. [19,22–25]

Compared to the other product layers, the YAP layer exhibits the strongest thickness variations, especially at long reaction times (>20 h). Its nucleation and growth depends on the growth and the grain boundary structure of both, the YAM and YAG product layers, as it is embedded between them. Thus, it may be caused by an increased variety of crystallite orientations in the YAM and YAG product layer compared to the single crystalline substrate or the initial Y_3O_3 thin film (see above), resulting in locally (more) different conditions for the growth of the YAP layer. When considering the weak contrasts due to channeling contrast in Figs. 6 and 7, there is (mainly) columnar grain growth in the YAG and YAM phases.

The observed pore formation in the interface between the Y_2O_3 and YAM phase, respectively in the bulk of the Y_2O_3 phase is most probably due to the presence of electronic conductivity at the high reaction temperature. As reported by Schmalzried and Pfeiffer, a running solid state reaction will cause a build-up of an oxygen partial pressure gradient in the presence of electronic conductivity, resulting in the formation of voids at grain and phase boundaries. [26]

5.3. *Growth kinetics, "practical" parabolic rate constants*

The data for the thickness increases of all three product layers can be sufficiently fitted by using the parabolic growth laws, see the dashed lines in Fig. 8. In the double logarithmic plot, diffusion-limited growth according Eq. (11) to (13) would correspond to straight lines with a slope of 1/2. In the case of the YAM product phase, slight systematical derivations towards higher values are visible at low layer thicknesses and in the case of the YAP product phase, towards lower values. A deviation in the low layer thicknesses may be caused by a change in the rate determining process from diffusion-limitation to an interface (transfer-) limitation. [22,23,27] In a double logarithmic plot the latter would correspond to a slope of 1. A decisive explanation is difficult, as the scattering of the data due to the uneven interfaces is in the same order, especially in the case of the YAP layer. It is only partially represented by the error bars. The uneven interfaces are primarily caused by a preferred nucleation of the product phases at the grain bondaries in the adjacent phases, as well as an enhanced grow in the vicinity of the interfaces, as they usually act as fast diffusion paths.

Despite the scattering of the data, especially for very thin layers, the expected diffusion-limitated growth kinetics (parabolic rate law) can be demonstrated. The following values for the "practical" parabolic rate constants of the reaction between Y_2O_3 and Al_2O_3 at 1400 are obtained by fitting with Eq. (11) to (13):

$$k'_{mM} = (1.15 \pm 0.07) \cdot 10^{-13}\ \mathrm{cm^2 s^{-1}}$$
$$k'_{P} = (1.32 \pm 0.18) \cdot 10^{-14}\ \mathrm{cm^2 s^{-1}}$$
$$k'_{G} = (4.51 \pm 0.32) \cdot 10^{-13}\ \mathrm{cm^2 s^{-1}}$$

The highest value for the "practical" parabolic rate constant can be found in the YAG phase. The kinetics of the YAP phase formation is about one order of magnitude slower compared to the other.

The simultaneous formation of multiple product phases has been reported by studies on powdery samples as well as on Y_2O_3 thin film samples on single crystalline Al_2O_3 substrates. According to studies using thin films on single crystalline substrates, the YAM phase appears first at the lowest experimental temperatures. [10–12] Using spin-coated samples and XRD for the analysis, Arakawa et al. detects the only formation of the YAM phase after a reaction time of 10 min. in the temperature range of 1000–1200 °C. Using samples prepared by PLD and TEM/SAED for the analysis, Heffelfinger et al. observe the only formation of an about 25 nm thick YAM layer after 6 h at 1200 °C. A lower limit for the reaction at 1100 °C is reported.

The simultaneous formation of the YAG and YAM phase were observed by Heffelfinger et al. after 6 h at a temperature of 1250 °C. An approximately 75 nm thick YAG and a 50 nm thick YAM layer were formed. The YAP phase was not detectable. Arakawa et al. were able to simultaneously detect the YAG, YAP and YAM phase above a reaction temperature of 1300 °C. In addition, they found a hexagonal modification of $YAlO_3$ (YAH) as fourth product phase above a reaction temperature of 1200 °C. This was also confirmed by Gandhi et al. for the reaction of powdery samples at 1250 °C. [6] A fourth product layer could not be confirmed in this study, as it may not be discernable from the YAP phase when using SEM in BSE contrast mode. It was also not confirmed by Heffelfinger et al. using TEM/SAED.

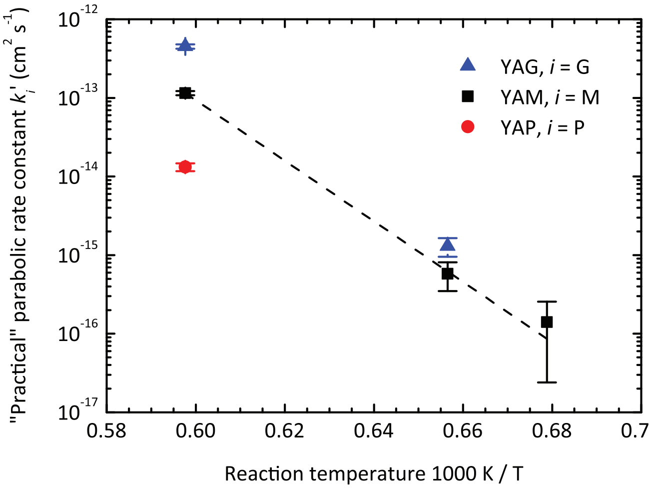

Fig. 9. Arrhenius plot of the "practical" parabolic rate constants k_i' (i = M, P and G) of the product layers YAG, YAP and YAM measured in this study and estimated from Heffelfinger et al. The dashed line is obtained by fitting the data of the YAM phase to the Arrhenius law.

Using the values for the product layer thickness of the YAM and YAG phase, evaluated from the TEM microslides provided in the publication by Heffelfinger et al., it is possible to estimate values for the "practical" parabolic rate constants at 1200 °C:

$$k'_{M} \approx 1.4 \cdot 10^{-16}\ \mathrm{cm^2 s^{-1}}\ \mathrm{for}\ (25 \pm 10)\,\mathrm{nm}/6\,\mathrm{h}$$

and at 1250 °C;

$$k'_{M} \approx 5.8 \cdot 10^{-16}\ \mathrm{cm^2 s^{-1}}\ \mathrm{for}\ (50 \pm 10)\,\mathrm{nm}/6\,\mathrm{h}$$
$$k'_{G} \approx 1.5 \cdot 10^{-15}\ \mathrm{cm^2 s^{-1}}\ \mathrm{for}\ (75 \pm 10)\,\mathrm{nm}/6\,\mathrm{h}$$

The available but very limited temperature-dependent data for the "practical" parabolic rate constants can be plotted in an Arrhenius diagram, see Fig. 9. However, despite these limitations, a fairly good fit is found in the case of the YAM phase (R^2 = 0.998). The "practical" parabolic rate constant k'_M of the YAM phase exhibits an activation energy of about 738 kJ mol^{-1} (7.6 eV). This is a considerably high value, but according to Eq. (A.66) to (A.68) and (A.78) to (A.80), k_M' is a weighted average of the (coupled) ionic conductivities of the YAM and YAP phases, as well as of the free formation enthalpies of both phases. The activation energies for ionic transport in YAM, YAP and YAG are (presumably) also considerably high. In a study by Bates and Garnier, a value of 3.4 eV could be found for single cystalline YAG (1000–1260 K). [28]

A simple approach to explain the absence of the YAP phase in the study of Heffelfinger et al. at a reaction temperature of 1250 °C and below is to estimate the "practical" parabolic rate constant k_P' for this temperature using Fig. 9. This is highly speculative, as the activation energy of k_P' is unknown. Assuming a comparable temperature dependence as that found for k_M', a value for k_P' in the order of 10^{-16} cm^2 s^{-1} seems reasonable. However, this may result in a YAP layer with a thickness of about 20 nm after 6 h reaction time. Thus, considerably different nucleation energies must also be taken into account. Just from the observed sequence a distinct product phase appears *vs.* the reaction temperature, one may assume that the nucleation energy is increasing in the order YAM < YAG < YAP.

According to the findings of the studies using powdery samples and diffraction methods, the reaction between Al_2O_3 and Y_2O_3 starts at temperatures of 1000–1200 °C. [6,7] A preferential formation of the YAM phase in the very beginning at low reaction temperatures is not reported.

5.4. Growth kinetics, “true” parabolic rate constants

The “true” parabolic rate constants for the independent and uncoupled growth of the product phases can be calculated by using Eq. (14) to (16) and values for the molar volumes. The required molar volumes V_m^M, V_m^P and V_m^G of the product phases were calculated by using the densities obtained from XRD data.[1] [29–32] This yields for the reaction temperature of 1400 °C:

$$k_M = (6.30 \pm 0.49)\cdot 10^{-13}\ \mathrm{cm^2 s^{-1}}$$
$$k_P = (3.04 \pm 0.34)\cdot 10^{-13}\ \mathrm{cm^2 s^{-1}}$$
$$k_G = (1.53 \pm 0.12)\cdot 10^{-12}\ \mathrm{cm^2 s^{-1}}$$

The differences between the “true” parabolic rate constants are clearly smaller compared to the “practical” constants. The observed slow kinetics of the YAP phase formation is mainly caused by the simultaneous consumption due to the YAG and YAM phase formation.

Considering Eq. (A.66) to (A.68) from the Appendix A, the molar volumes and the standard free formation enthalpies of the product phases, it is possible to estimate the Nernst-Planck-coupled cation partial conductivities in the product layers. This yields:

$$\frac{\sigma^M_{Y^{3+}}\sigma^M_{Al^{3+}}}{\sigma^M_{Y^{3+}} + \sigma^M_{Al^{3+}}} = (8.92 \pm 0.70)\cdot 10^{-9}\ \mathrm{S\,cm^{-1}}$$

$$\frac{\sigma^P_{Y^{3+}}\sigma^P_{Al^{3+}}}{\sigma^P_{Y^{3+}} + \sigma^P_{Al^{3+}}} = (2.3 \pm 1.4)\cdot 10^{-9}\ \mathrm{S\,cm^{-1}}$$

$$\frac{\sigma^G_{Y^{3+}}\sigma^G_{Al^{3+}}}{\sigma^G_{Y^{3+}} + \sigma^G_{Al^{3+}}} = (3.55 \pm 0.23)\cdot 10^{-8}\ \mathrm{S\,cm^{-1}}$$

The required values for the standard free formation enthalpies $\Delta_R G^\circ_M$, $\Delta_R G^\circ_P$ and $\Delta_R G^\circ_G$ can be calculated from data given by Fabrichnaya et al.[2] [33,34] The highest (Nernst-Planck averaged) cation conductivity is found in the garnet phase, the lowest in the perovskite phase. This resembles also the observed product phase thicknesses.

Only very few measurments have been made of the ionic conductivies of the product phases. A value of the total ionic conductivity for the YAG phase at 1400 °C, $\sigma^G_{tot} \approx 6.3\cdot 10^{-7}$ S cm^{-1}, can be gained from a study by Bates and Garnier. [28] Taking the experimental setup into account and neglecting a possible O^{2-} anion and electronic conductivity, the given value is presumably the total cationic conductivity $\sigma_{Y^{3+}}{}^{G} + \sigma_{Al^{3+}}{}^{G}$. This was also suggested by Bates and Garnier, attributing the conductivity mainly to the Al^{3+} cations. Using the Nernst-Planck-coupled cation conductivity from this study and the total cation conductivity from Bates and Garnier, it is possible to estimate values for the cation partial conductivities in the YAG phase[3]:

$$\sigma^G_{Y^{3+}} \approx 3.8\cdot 10^{-8}\ \mathrm{S\,cm^{-1}}$$
$$\sigma^G_{Al^{3+}} \approx 5.9\cdot 10^{-7}\ \mathrm{S\,cm^{-1}}$$

This yields a transference number for the Al^{3+} cations of $t_{Al^{3+}}{}^{G} \approx 0.94$ and would confirm the former assumptions of Bates and Garnier.

Eq. (A.66) to (A.68) which are used to calculate the “true” parabolic rate constants are derived by neglecting a possible contribution due to O^{2-} ion conduction to the product phase growth. An additional contribution due to an O^{2-} ion flux would also lead to a parabolic growth law. It would change the expected relative shifts of the reaction fronts (phase boundaries) in relation to a fixed reference frame, *e.g.* to the lattice of the Al_2O_3 substrate, respectively to the original position of the interface to the Y_2O_3 thin film. The relative shift (velocities) of the phase boundaries of, *e.g.* the garnet phase, can be derived from Eq. (A.8) and (A.9) by combining with (A.29), (A.32), (A.56) and (A.59). The original interface between the substrate and the reacting film can be principally marked by embedding platinum particle. [25] Unfortunately, this was not performed for the complex reaction system in this study. Thus, the (coupled) cationic conductivities in Eq. (5.4) to (5.4) may be overestimated.

6. Summary

The formalisms of Wagner and Schmalzried is applied for the general treatment of the solid state reaction in the Al_2O_3–Y_2O_3 system using linear transport theory. In the case of the simultaneous formation of multiple product phases “practical” and “true” parabolic rate constants must be distinguished.

The “practical” parabolic rate constants for the simultaneous growth of the three product phases YAM, YAP and YAM are determined for a reaction temperature of 1400 °C. The growth kinetics of all product phases can be satisfactorily described by parabolic rate law (Tammann law). There are possibly small derivations for layer thicknesses below 5 nm. When evaluating experimental studies from the literature performed at lower reaction temperatures, it is possible to estimate the activation energy of the “practical” parabolic rate constant of the YAM phase. The obtained high value may represent the high activation energies for ionic transport in this material. The combined data of this study and of that by Heffelfinger et al. performed on geometrical defined thin film samples helps illuminate the reaction kinetics of the Al_2O_3-–Y_2O_3 system in the temperature range between 1200 and 1400 °C. At a low reaction temperature of 1200 °C, the nucleation of the product phases is strongly influenced by the (presumably) different nucleation energies.

The “true” parabolic rate constants are calculated from measured data using a model for the product phase growth based on linear transport theory. Using caloric data from the literature, it is possible to calculate the Nernst-Planck-coupled cation partial conductivities of all product phases. Using the total ionic conductivity of the YAG phase from the literature it is possible to estimate the cationic transference numbers.

Declaration of Competing Interest

The authors declare that they have no known competing financial interests or personal relationships that could have appeared to influence the work reported in this paper.

---

[1] YAM phase: $V_m^M = 122.88$ cm^3 mol^{-1}, YAP phase: $V_m^P = 30.66$ cm^3 mol^{-1} and YAG phase: $V_m^G = 130.37$ cm^3 mol^{-1}

[2] Fabrichnaya et al. reviewed the available thermochemical data of the Al_2O_3–Y_2O_3 system from various sources and performed thermochemical calculations of the phase diagram using the calphad approach. Experimental data for the standard free formation enthalpies of YAM, YAP and YAG from the binary oxides Al_2O_3 and Y_2O_3 at 1350 K is given, see Eq. (A.18) to (A.20) from Appendix A:

$$\Delta_f G^\circ_M = -67.6\ \mathrm{kJ\,mol^{-1}}$$
$$\Delta_f G^\circ_P = -23.1\ \mathrm{kJ\,mol^{-1}}$$
$$\Delta_f G^\circ_G = -84.9\ \mathrm{kJ\,mol^{-1}}$$

The values are increasing with increasing temperature. At the reaction temperature of 1673 K (1400 °C) used in this study the values measured at 1350 K may deviate by no more than 10%. Using Eq. (A.45) to (A.47) from the Appendix A to calculate the standard free formation enthalpies $\Delta_R G^\circ_M$, $\Delta_R G^\circ_P$ and $\Delta_R G^\circ_G$ yields:

$$\Delta_R G^\circ_M = -21.5\ \mathrm{kJ\,mol^{-1}}$$
$$\Delta_R G^\circ_P = -7,33\ \mathrm{kJ\,mol^{-1}}$$
$$\Delta_R G^\circ_G = -15,8\ \mathrm{kJ\,mol^{-1}}$$

[3] There is also a second set of solutions with reversed conductivity values for the cations as the problem yields a quadratic equation. The second set would imply a higher (but improbable) conductivity of Y^{3+} cations, *i.e.* $\sigma_{Y^{3+}}{}^{G} \gg \sigma_{Al^{3+}}{}^{G}$.

Acknowledgment

We are grateful to the German Science Foundation (DFG, Ko1859/2-1) and the State of Hessen for financial support (BF and CK).

Appendix A. Description of the heterogenoues reaction system A_2O_3–B_2O_3 by linear transport theory

The following treatment is restricted to a one-dimensional system, see Fig. 1. For the sake of simplicity all vector quantities as the (ionic) fluxes, (phase boundary) velocities and electrochemical potential gradients will be introduced as scalars. A positive sign corresponds to a vector in the direction of the *x*-axis and a negative to a vector in the opposite direction.

A.1. Condition of electroneutrality

All of the cation fluxes in the three product phases M, P and G are coupled by the condition of electroneutrality, *i.e.* Nernst-Planck coupling:

$$\mathrm{M}:\; j^{\mathrm{M}}_{\mathrm{A}^{3+}} + j^{\mathrm{M}}_{\mathrm{B}^{3+}} = 0 \tag{A.1}$$

$$\mathrm{P}:\; j^{\mathrm{P}}_{\mathrm{A}^{3+}} + j^{\mathrm{P}}_{\mathrm{B}^{3+}} = 0 \tag{A.2}$$

$$\mathrm{G}:\; j^{\mathrm{G}}_{\mathrm{A}^{3+}} + j^{\mathrm{G}}_{\mathrm{B}^{3+}} = 0 \tag{A.3}$$

The presence of O^{2-} and electronic fluxes would lead to a decoupling of the cation fluxes in Eq. (A.1) to (A.3). This would (partially) cancel the Nernst-Planck coupling. Furthermore, it would modified the partial reactions at the interfaces in Eq. (5) to (7), now including oxide ions as reaction partner.

A.2. Velocity of the phase boundaries (reaction front)

When regarding the stoichiometric factors in Eq. (7), (6), (5) and (4) the movements of the phase boundaries can be expressed by the cation fluxes in the product layers. The oxide sublattices of the product phases will be assumed as rigid reference frames. The movement of each phase boundary/reaction front can be described as velocities relative to the adjoining phases, which are not necessarily the same, as the molar volumes of the product phases are different:

$$\mathrm{M}:\; v^{\mathrm{M}}_{\mathrm{P/M}} = V^{\mathrm{M}}_{\mathrm{m}}\left(j^{\mathrm{M}}_{\mathrm{A}^{3+}} - j^{\mathrm{P}}_{\mathrm{A}^{3+}}\right) = -V^{\mathrm{M}}_{\mathrm{m}}\left(j^{\mathrm{M}}_{\mathrm{B}^{3+}} - j^{\mathrm{P}}_{\mathrm{B}^{3+}}\right) \tag{A.4}$$

$$v^{\mathrm{M}}_{\mathrm{M/A_2O_3}} = -\frac{1}{2}V^{\mathrm{M}}_{\mathrm{m}} j^{\mathrm{M}}_{\mathrm{A}^{3+}} = \frac{1}{2}V^{\mathrm{M}}_{\mathrm{m}} j^{\mathrm{M}}_{\mathrm{B}^{3+}} \tag{A.5}$$

$$\mathrm{P}:\; v^{\mathrm{P}}_{\mathrm{G/P}} = 4V^{\mathrm{P}}_{\mathrm{m}}\left(j^{\mathrm{P}}_{\mathrm{A}^{3+}} - j^{\mathrm{G}}_{\mathrm{A}^{3+}}\right) = -4V^{\mathrm{P}}_{\mathrm{m}}\left(j^{\mathrm{P}}_{\mathrm{B}^{3+}} - j^{\mathrm{G}}_{\mathrm{B}^{3+}}\right) \tag{A.6}$$

$$v^{\mathrm{P}}_{\mathrm{P/M}} = 3V^{\mathrm{P}}_{\mathrm{m}}\left(j^{\mathrm{M}}_{\mathrm{A}^{3+}} - j^{\mathrm{P}}_{\mathrm{A}^{3+}}\right) = -3V^{\mathrm{P}}_{\mathrm{m}}\left(j^{\mathrm{M}}_{\mathrm{B}^{3+}} - j^{\mathrm{P}}_{\mathrm{B}^{3+}}\right) \tag{A.7}$$

$$\mathrm{G}:\; v^{\mathrm{G}}_{\mathrm{B_2O_3/G}} = \frac{1}{3}V^{\mathrm{G}}_{\mathrm{m}} j^{\mathrm{G}}_{\mathrm{A}^{3+}} = -\frac{1}{3}V^{\mathrm{G}}_{\mathrm{m}} j^{\mathrm{G}}_{\mathrm{B}^{3+}} \tag{A.8}$$

$$v^{\mathrm{G}}_{\mathrm{G/P}} = V^{\mathrm{G}}_{\mathrm{m}}\left(j^{\mathrm{P}}_{\mathrm{A}^{3+}} - j^{\mathrm{G}}_{\mathrm{A}^{3+}}\right) = -V^{\mathrm{G}}_{\mathrm{m}}\left(j^{\mathrm{P}}_{\mathrm{B}^{3+}} - j^{\mathrm{G}}_{\mathrm{B}^{3+}}\right) \tag{A.9}$$

Hereby, ${v_{\mathrm{M/A_2O_3}}}^{\mathrm{M}}$ and $v^{\mathrm{M}}_{\mathrm{P/M}}$ are the relative velocities of the phase boundaries M/A_2O_3 and P/M with respect to the rigid oxide sublattice of the monoclinic phase (M), $v^{\mathrm{P}}_{\mathrm{P/M}}$ and $v^{\mathrm{P}}_{\mathrm{G/P}}$ the relative velocities of the phase boundaries P/M und G/P with respect to the perowskite phase (P), respectively $v^{\mathrm{G}}_{\mathrm{G/P}}$ and ${v_{\mathrm{B_2O_3/G}}}^{\mathrm{G}}$ the relative velocities of the phase boundaries G/P und B_2O_3/G with respect to the garnet phase (G). The molar volumes of the product phases M, P and G are denoted with $V^{\mathrm{M}}_{\mathrm{m}}$, $V^{\mathrm{P}}_{\mathrm{m}}$ and $V^{\mathrm{G}}_{\mathrm{m}}$.

The rate of the thickness change of a distinct product phase can be obtained from the difference of the relative phase boundary velocities belonging to that phase:

$$\mathrm{M}:\; \frac{\mathrm{d}(\Delta x_{\mathrm{M}})}{\mathrm{d}t} = v^{\mathrm{M}}_{\mathrm{M/A_2O_3}} - v^{\mathrm{M}}_{\mathrm{P/M}} \tag{A.10}$$

$$\mathrm{P}:\; \frac{\mathrm{d}(\Delta x_{\mathrm{P}})}{\mathrm{d}t} = v^{\mathrm{P}}_{\mathrm{P/M}} - v^{\mathrm{P}}_{\mathrm{G/P}} \tag{A.11}$$

$$\mathrm{G}:\; \frac{\mathrm{d}(\Delta x_{\mathrm{G}})}{\mathrm{d}t} = v^{\mathrm{G}}_{\mathrm{G/P}} - v^{\mathrm{G}}_{\mathrm{B_2O_3/G}} \tag{A.12}$$

Combining Eq. (A.10) to (A.12) with Eq. (A.4) to (A.9) yields:

$$\mathrm{M}:\; \frac{1}{V^{\mathrm{M}}_{\mathrm{m}}}\frac{\mathrm{d}(\Delta x_{\mathrm{M}})}{\mathrm{d}t} = -\left(\frac{3}{2}j^{\mathrm{M}}_{\mathrm{A}^{3+}} - j^{\mathrm{P}}_{\mathrm{A}^{3+}}\right) = \frac{3}{2}j^{\mathrm{M}}_{\mathrm{B}^{3+}} - j^{\mathrm{P}}_{\mathrm{B}^{3+}} \tag{A.13}$$

$$\mathrm{P}:\; \frac{1}{V^{\mathrm{P}}_{\mathrm{m}}}\frac{\mathrm{d}(\Delta x_{\mathrm{P}})}{\mathrm{d}t} = 3j^{\mathrm{M}}_{\mathrm{A}^{3+}} - 7j^{\mathrm{P}}_{\mathrm{A}^{3+}} + 4\overrightarrow{j}^{\mathrm{G}}_{\mathrm{A}^{3+}} = -\left(3j^{\mathrm{M}}_{\mathrm{B}^{3+}} - 7j^{\mathrm{P}}_{\mathrm{B}^{3+}} + 4j^{\mathrm{G}}_{\mathrm{B}^{3+}}\right) \tag{A.14}$$

$$\mathrm{G}: \ \frac{1}{V_\mathrm{m}^\mathrm{G}} \frac{\mathrm{d}(\Delta x_\mathrm{G})}{\mathrm{d}t} = j_{\mathrm{A}^{3+}}^\mathrm{P} - \frac{4}{3} j_{\mathrm{A}^{3+}}^\mathrm{G} = -\left(j_{\mathrm{B}^{3+}}^\mathrm{P} - \frac{4}{3} j_{\mathrm{B}^{3+}}^\mathrm{G} \right) \tag{A.15}$$

A.3. Diffusive charge transport

In all three product phases M, P and G, the ionic transport is driven by chemical potential gradients and can be described by linear transport equations (with $i = $ M,P or G):

$$j_{\mathrm{A}^{3+}}^i = -\frac{\sigma_{\mathrm{A}^{3+}}^i}{(3F)^2} \frac{\mathrm{d}\widetilde{\mu}_{\mathrm{A}^{3+}}^i}{\mathrm{d}x} \tag{A.16}$$

$$j_{\mathrm{B}^{3+}}^i = -\frac{\sigma_{\mathrm{B}^{3+}}^i}{(3F)^2} \frac{\mathrm{d}\widetilde{\mu}_{\mathrm{B}^{3+}}^i}{\mathrm{d}x} \tag{A.17}$$

Hereby, ${\sigma_{\mathrm{A}^{3+}}}^i$ and ${\sigma_{\mathrm{B}^{3+}}}^i$ are the partial cation conductivities in all product phases i. For the further treatment the electrochemical potential gradients $\mathrm{d}\widetilde{\mu}_{\mathrm{A}^{3+}}^i/\mathrm{d}x$ and $\mathrm{d}\widetilde{\mu}_{\mathrm{B}^{3+}}^i/\mathrm{d}x$ of the cations have to be expressed by directly measurable values as the chemical potential gradients of components A_2O_3 and B_2O_3, respectively by their differences. The chemical potential gradients of the components A_2O_3 und B_2O_3 are coupled necessarily in each product phase. When considering the formation of each product phases from the components A_2O_3 and B_2O_3, this will lead to the following relations for the bulk of the monoclinic (M), the perovskite (P) and the garnet phase (G)[4]:

$$\mathrm{M}: \ 2\frac{\mathrm{d}\mu_{\mathrm{A_2O_3}}^\mathrm{M}}{\mathrm{d}x} + \frac{\mathrm{d}\mu_{\mathrm{B_2O_3}}^\mathrm{M}}{\mathrm{d}x} = 0 \tag{A.21}$$

$$\mathrm{P}: \ \frac{\mathrm{d}\mu_{\mathrm{A_2O_3}}^\mathrm{P}}{\mathrm{d}x} + \frac{\mathrm{d}\mu_{\mathrm{B_2O_3}}^\mathrm{P}}{\mathrm{d}x} = 0 \tag{A.22}$$

$$\mathrm{G}: \ 3\frac{\mathrm{d}\mu_{\mathrm{A_2O_3}}^\mathrm{G}}{\mathrm{d}x} + 5\frac{\mathrm{d}\mu_{\mathrm{B_2O_3}}^\mathrm{G}}{\mathrm{d}x} = 0 \tag{A.23}$$

Taking Eq. (A.21), (A.22) and (A.23) into account, it is also possible to derive a coupling between the electrochemical potential gradients of A^{3+} and B^{3+} cations in each product phase:

$$\mathrm{M}: \ \frac{\mathrm{d}\widetilde{\mu}_{\mathrm{A}^{3+}}^\mathrm{M}}{\mathrm{d}x} - \frac{\mathrm{d}\widetilde{\mu}_{\mathrm{B}^{3+}}^\mathrm{M}}{\mathrm{d}x} = \frac{1}{2}\left(\frac{\mathrm{d}\mu_{\mathrm{A_2O_3}}^\mathrm{M}}{\mathrm{d}x} - \frac{\mathrm{d}\mu_{\mathrm{B_2O_3}}^\mathrm{M}}{\mathrm{d}x} \right) = \frac{3}{2}\frac{\mathrm{d}\mu_{\mathrm{A_2O_3}}^\mathrm{M}}{\mathrm{d}x} = -\frac{3}{4}\frac{\mathrm{d}\mu_{\mathrm{B_2O_3}}^\mathrm{M}}{\mathrm{d}x} \tag{A.24}$$

$$\mathrm{P}: \ \frac{\mathrm{d}\widetilde{\mu}_{\mathrm{A}^{3+}}^\mathrm{P}}{\mathrm{d}x} - \frac{\mathrm{d}\widetilde{\mu}_{\mathrm{B}^{3+}}^\mathrm{P}}{\mathrm{d}x} = \frac{\mathrm{d}\mu_{\mathrm{A_2O_3}}^\mathrm{P}}{\mathrm{d}x} = -\frac{\mathrm{d}\mu_{\mathrm{B_2O_3}}^\mathrm{P}}{\mathrm{d}x} \tag{A.25}$$

$$\mathrm{G}: \ \frac{\mathrm{d}\widetilde{\mu}_{\mathrm{A}^{3+}}^\mathrm{G}}{\mathrm{d}x} - \frac{\mathrm{d}\widetilde{\mu}_{\mathrm{B}^{3+}}^\mathrm{G}}{\mathrm{d}x} = \frac{4}{5}\frac{\mathrm{d}\mu_{\mathrm{A_2O_3}}^\mathrm{G}}{\mathrm{d}x} = -\frac{4}{3}\frac{\mathrm{d}\mu_{\mathrm{B_2O_3}}^\mathrm{G}}{\mathrm{d}x} \tag{A.26}$$

Using Eq. (A.24), (A.25) and (A.26) and the coupling of the cation fluxes in each product phase due to electroneutrality in Eq. (A.1), (A.2) and (A.3), the relations between the electrochemical potential gradients of the cations and the chemical potential gradients of the components A_2O_3 and B_2O_3 can be derived. Thus, the cation fluxes in Eq. (A.16) and (A.17) can be rewritten that only the chemical potential gradients of the components A_2O_3 and B_2O_3 appear as driving forces:

$$\mathrm{M}: \ j_{\mathrm{A}^{3+}}^\mathrm{M} = -\frac{3}{2}\frac{1}{(3F)^2}\frac{\sigma_{\mathrm{A}^{3+}}^\mathrm{M}\sigma_{\mathrm{B}^{3+}}^\mathrm{M}}{\sigma_{\mathrm{A}^{3+}}^\mathrm{M} + \sigma_{\mathrm{B}^{3+}}^\mathrm{M}}\frac{d\mu_{\mathrm{A_2O_3}}^\mathrm{M}}{dx} \tag{A.27}$$

$$j_{\mathrm{B}^{3+}}^\mathrm{M} = -\frac{3}{4}\frac{1}{(3F)^2}\frac{\sigma_{\mathrm{A}^{3+}}^\mathrm{M}\sigma_{\mathrm{B}^{3+}}^\mathrm{M}}{\sigma_{\mathrm{A}^{3+}}^\mathrm{M} + \sigma_{\mathrm{B}^{3+}}^\mathrm{M}}\frac{d\mu_{\mathrm{B_2O_3}}^\mathrm{M}}{dx} \tag{A.28}$$

$$\mathrm{P}: \ j_{\mathrm{A}^{3+}}^\mathrm{P} = -\frac{1}{(3F)^2}\frac{\sigma_{\mathrm{A}^{3+}}^\mathrm{P}\sigma_{\mathrm{B}^{3+}}^\mathrm{P}}{\sigma_{\mathrm{A}^{3+}}^\mathrm{P} + \sigma_{\mathrm{B}^{3+}}^\mathrm{P}}\frac{d\mu_{\mathrm{A_2O_3}}^\mathrm{P}}{dx} \tag{A.29}$$

$$j_{\mathrm{B}^{3+}}^\mathrm{P} = -\frac{1}{(3F)^2}\frac{\sigma_{\mathrm{A}^{3+}}^\mathrm{P}\sigma_{\mathrm{B}^{3+}}^\mathrm{P}}{\sigma_{\mathrm{A}^{3+}}^\mathrm{P} + \sigma_{\mathrm{B}^{3+}}^\mathrm{P}}\frac{d\mu_{\mathrm{B_2O_3}}^\mathrm{P}}{dx} \tag{A.30}$$

---

[4] Total reactions to form the products M, P and G directly from the components A_2O_3 and B_2O_3:

$$2A_2O_3 + B_2O_3 = A_4B_2O_9 \tag{A.18}$$

$$A_2O_3 + B_2O_3 = 2ABO_3 \tag{A.19}$$

$$3A_2O_3 + 5B_2O_3 = 2A_3B_5O_{12} \tag{A.20}$$

$$\mathrm{G}:\ j^{\mathrm{G}}_{\mathrm{A}^{3+}} = -\frac{4}{5}\frac{1}{(3F)^2}\frac{\sigma^{\mathrm{G}}_{\mathrm{A}^{3+}}\sigma^{\mathrm{G}}_{\mathrm{B}^{3+}}}{\sigma^{\mathrm{G}}_{\mathrm{A}^{3+}}+\sigma^{\mathrm{G}}_{\mathrm{B}^{3+}}}\frac{d\mu^{\mathrm{G}}_{\mathrm{A_2O_3}}}{dx} \tag{A.31}$$

$$j^{\mathrm{G}}_{\mathrm{B}^{3+}} = -\frac{4}{3}\frac{1}{(3F)^2}\frac{\sigma^{\mathrm{G}}_{\mathrm{A}^{3+}}\sigma^{\mathrm{G}}_{\mathrm{B}^{3+}}}{\sigma^{\mathrm{G}}_{\mathrm{A}^{3+}}+\sigma^{\mathrm{G}}_{\mathrm{B}^{3+}}}\frac{d\mu^{\mathrm{G}}_{\mathrm{B_2O_3}}}{dx} \tag{A.32}$$

A.4. *Chemical potential gradients of the components A_2O_3 and B_2O_3 in the product layers*

The chemical potentials of the components A_2O_3 and B_2O_3 at the boundaries between a product layer can be derived from the chemical equilibria[5]:

$$\mathrm{M}\Big/\mathrm{A_2O_3}:\ \mu^{\mathrm{M/A_2O_3}}_{\mathrm{A_2O_3}} = \mu^0_{\mathrm{A_2O_3}} \tag{A.37}$$

$$\mu^{\mathrm{M/A_2O_3}}_{\mathrm{B_2O_3}} = \mu^0_{\mathrm{A_4B_2O_9}} - 2\mu^0_{\mathrm{A_2O_3}} \tag{A.38}$$

$$\mathrm{P}\Big/\mathrm{M}:\ \mu^{\mathrm{P/M}}_{\mathrm{A_2O_3}} = \mu^0_{\mathrm{A_4B_2O_9}} - 2\mu^0_{\mathrm{ABO_3}} \tag{A.39}$$

$$\mu^{\mathrm{P/M}}_{\mathrm{B_2O_3}} = 4\mu^0_{\mathrm{ABO_3}} - \mu^0_{\mathrm{A_4B_2O_9}} \tag{A.40}$$

$$\mathrm{G}\Big/\mathrm{P}:\ \mu^{\mathrm{G/P}}_{\mathrm{A_2O_3}} = 5\mu^0_{\mathrm{ABO_3}} - \mu^0_{\mathrm{A_3B_5O_{12}}} \tag{A.41}$$

$$\mu^{\mathrm{G/P}}_{\mathrm{B_2O_3}} = \mu^0_{\mathrm{A_3B_5O_{12}}} - 3\mu^0_{\mathrm{ABO_3}} \tag{A.42}$$

$$\mathrm{B_2O_3}\Big/\mathrm{G}:\ \mu^{\mathrm{B_2O_3/G}}_{\mathrm{A_2O_3}} = 2\Big/3\mu^0_{\mathrm{A_3B_5O_{12}}} - 5\Big/3\mu^0_{\mathrm{B_2O_3}} \tag{A.43}$$

$$\mu^{\mathrm{B_2O_3/G}}_{\mathrm{B_2O_3}} = \mu^0_{\mathrm{B_2O_3}} \tag{A.44}$$

The free reaction enthalpies $\Delta_R G^\circ_M$, $\Delta_R G^\circ_P$ and $\Delta_R G^\circ_G$ for the partial reaction in Eq. (1), (2) and (3) are defined as follows[6]:

$$\Delta_{\mathrm{R}}G^\circ_{\mathrm{M}} = \mu^0_{\mathrm{A_4B_2O_9}} - \left(\mu^0_{\mathrm{A_2O_3}} + 2\mu^0_{\mathrm{ABO_3}}\right) \tag{A.51}$$

$$\Delta_{\mathrm{R}}G^\circ_{\mathrm{P}} = \mu^0_{\mathrm{ABO_3}} - \frac{1}{7}\left(\mu^0_{\mathrm{A_4B_2O_9}} + \mu^0_{\mathrm{A_3B_5O_{12}}}\right) \tag{A.52}$$

$$\Delta_{\mathrm{R}}G^\circ_{\mathrm{G}} = \mu^0_{\mathrm{A_3B_5O_{12}}} - \left(3\mu^0_{\mathrm{ABO_3}} + \mu^0_{\mathrm{B_2O_3}}\right) \tag{A.53}$$

The chemical potential gradients of the components A_2O_3 and B_2O_3 in each product layer can be calculated from the difference of the component

---

[5] Chemical equilibria of components A_2O_3 and B_2O_3 at the phase boundaries:

$$\mathrm{M/A_2O_3}: \mathrm{A_4B_2O_9} = 2\mathrm{A_2O_3} + \mathrm{B_2O_3} \tag{A.33}$$

$$\begin{aligned}\mathrm{P/M}: 2\mathrm{ABO_3} + \mathrm{A_2O_3} &= \mathrm{A_4B_2O_9}\\ 4\mathrm{ABO_3} &= \mathrm{A_4B_2O_9} + \mathrm{B_2O_3}\end{aligned} \tag{A.34}$$

$$\begin{aligned}\mathrm{G/P}: \mathrm{A_3B_5O_{12}} + \mathrm{A_2O_3} &= 5\mathrm{ABO_3}\\ \mathrm{A_3B_5O_{12}} &= 3\mathrm{ABO_3} + \mathrm{B_2O_3}\end{aligned} \tag{A.35}$$

$$\mathrm{B_2O_3/G}: 5\mathrm{B_2O_3} + 3\mathrm{A_2O_3} = 2\mathrm{A_3B_5O_{12}} \tag{A.36}$$

[6] The free reaction enthalpies $\Delta_R G^\circ_M$, $\Delta_R G^\circ_P$ and $\Delta_R G^\circ_G$ of the partial reaction in Eq. (1), (2) and (3) can be expressed by the free reaction enthalpies $\Delta_f G^\circ_M$, $\Delta_f G^\circ_P$ and $\Delta_f G^\circ_G$ for the formation of the product phase directly from the components A_2O_3 and B_2O_3 in Eq. (A.18), (A.19) and (A.20):

$$\Delta_{\mathrm{R}}G^\circ_{\mathrm{M}} = \Delta_{\mathrm{f}}G^\circ_{\mathrm{M}} - 2\Delta_{\mathrm{f}}G^\circ_{\mathrm{P}} \tag{A.45}$$

$$\Delta_{\mathrm{R}}G^\circ_{\mathrm{P}} = \Delta_{\mathrm{f}}G^\circ_{\mathrm{P}} - 1/7\left(\Delta_{\mathrm{f}}G^\circ_{\mathrm{M}} + 1/2\Delta_{\mathrm{f}}G^\circ_{\mathrm{G}}\right) \tag{A.46}$$

$$\Delta_{\mathrm{R}}G^\circ_{\mathrm{G}} = \Delta_{\mathrm{f}}G^\circ_{\mathrm{G}} - 3\Delta_{\mathrm{f}}G^\circ_{\mathrm{P}} \tag{A.47}$$

$$\Delta_{\mathrm{f}}G^\circ_{\mathrm{M}} = \mu^0_{\mathrm{A_4B_2O_9}} - \left(2\mu^0_{\mathrm{A_2O_3}} + \mu^0_{\mathrm{B_2O_3}}\right) \tag{A.48}$$

$$\Delta_{\mathrm{f}}G^\circ_{\mathrm{P}} = \mu^0_{\mathrm{ABO_3}} - 1\Big/2\left(\mu^0_{\mathrm{A_2O_3}} + \mu^0_{\mathrm{B_2O_3}}\right) \tag{A.49}$$

$$\Delta_{\mathrm{f}}G^\circ_{\mathrm{G}} = \mu^0_{\mathrm{A_3B_5O_{12}}} - 1\Big/2\left(3\mu^0_{\mathrm{A_2O_3}} + 5\mu^0_{\mathrm{B_2O_3}}\right) \tag{A.50}$$

chemical potentials at the adjacent phase boundaries and the product layer thicknesses Δx_M, Δx_P and Δx_G. Thus, using Eq. (A.37) to (A.53), one obtains for the monoclinic phase (M) (*e.g.* $\Delta \mu_{\mathrm{A_2O_3}}{}^\mathrm{M} = \mu_{\mathrm{A_2O_3}}{}^{\mathrm{M/A_2O_3}} - \mu_{\mathrm{A_2O_3}}{}^{\mathrm{P/M}}$):

$$\frac{d\mu^\mathrm{M}_{\mathrm{A_2O_3}}}{dx} \approx \frac{\Delta\mu^\mathrm{M}_{\mathrm{A_2O_3}}}{\Delta x_\mathrm{M}} = -\frac{\Delta_\mathrm{R} G^\circ_\mathrm{M}}{\Delta x_\mathrm{M}} \tag{A.54}$$

$$\frac{d\mu^\mathrm{M}_{\mathrm{B_2O_3}}}{dx} \approx \frac{\Delta\mu^\mathrm{M}_{\mathrm{B_2O_3}}}{\Delta x_\mathrm{M}} = 2\frac{\Delta_\mathrm{R} G^\circ_\mathrm{M}}{\Delta x_\mathrm{M}} \tag{A.55}$$

for the perovskite phase (P):

$$\frac{d\mu^\mathrm{P}_{\mathrm{A_2O_3}}}{dx} \approx \frac{\Delta\mu^\mathrm{P}_{\mathrm{A_2O_3}}}{\Delta x_\mathrm{P}} = -7\frac{\Delta_\mathrm{R} G^\circ_\mathrm{P}}{\Delta x_\mathrm{P}} \tag{A.56}$$

$$\frac{d\mu^\mathrm{P}_{\mathrm{B_2O_3}}}{dx} \approx \frac{\Delta\mu^\mathrm{P}_{\mathrm{B_2O_3}}}{\Delta x_\mathrm{P}} = 7\frac{\Delta_\mathrm{R} G^\circ_\mathrm{P}}{\Delta x_\mathrm{P}} \tag{A.57}$$

and for the garnet phase (G):

$$\frac{d\mu^\mathrm{G}_{\mathrm{A_2O_3}}}{dx} \approx \frac{\Delta\mu^\mathrm{G}_{\mathrm{A_2O_3}}}{\Delta x_\mathrm{G}} = -\frac{5}{3}\frac{\Delta_\mathrm{R} G^\circ_\mathrm{G}}{\Delta x_\mathrm{G}} \tag{A.58}$$

$$\frac{d\mu^\mathrm{G}_{\mathrm{B_2O_3}}}{dx} \approx \frac{\Delta\mu^\mathrm{G}_{\mathrm{B_2O_3}}}{\Delta x_\mathrm{G}} = \frac{\Delta_\mathrm{R} G^\circ_\mathrm{G}}{\Delta x_\mathrm{G}} \tag{A.59}$$

A.5. Simultaneous growth of all product layers, "true" and "practical" Tammann rate constants

The results from the preceeding paragraphs regarding component gradients and cation fluxes can be combined to obtain expressions for the growth rates of each product layer. The rate equation for the growth of the monoclinic phase (M) in Eq. (A.60) can be acquired by using Eq. (A.13) and the cation fluxes in Eq. (A.27) to (A.30):

$$\begin{aligned}\frac{1}{V^\mathrm{M}_\mathrm{m}}\frac{\mathrm{d}(\Delta x_\mathrm{M})}{\mathrm{d}t} &= -\left(\frac{3}{2}j^\mathrm{M}_{\mathrm{A^{3+}}} - j^\mathrm{P}_{\mathrm{A^{3+}}}\right) = \frac{3}{2}j^\mathrm{M}_{\mathrm{B^{3+}}} - j^\mathrm{P}_{\mathrm{B^{3+}}} \\ &= \frac{1}{(3F)^2}\left[\frac{9}{4}\frac{\sigma^\mathrm{M}_{\mathrm{A^{3+}}}\sigma^\mathrm{M}_{\mathrm{B^{3+}}}}{\sigma^\mathrm{M}_{\mathrm{A^{3+}}}+\sigma^\mathrm{M}_{\mathrm{B^{3+}}}}\frac{d\mu^\mathrm{M}_{\mathrm{A_2O_3}}}{dx} - \frac{\sigma^\mathrm{P}_{\mathrm{A^{3+}}}\sigma^\mathrm{P}_{\mathrm{B^{3+}}}}{\sigma^\mathrm{P}_{\mathrm{A^{3+}}}+\sigma^\mathrm{P}_{\mathrm{B^{3+}}}}\frac{d\mu^\mathrm{P}_{\mathrm{A_2O_3}}}{dx}\right] = -\frac{1}{(3F)^2}\left[\frac{9}{8}\frac{\sigma^\mathrm{M}_{\mathrm{A^{3+}}}\sigma^\mathrm{M}_{\mathrm{B^{3+}}}}{\sigma^\mathrm{M}_{\mathrm{A^{3+}}}+\sigma^\mathrm{M}_{\mathrm{B^{3+}}}}\frac{d\mu^\mathrm{M}_{\mathrm{B_2O_3}}}{dx} - \frac{\sigma^\mathrm{P}_{\mathrm{A^{3+}}}\sigma^\mathrm{P}_{\mathrm{B^{3+}}}}{\sigma^\mathrm{P}_{\mathrm{A^{3+}}}+\sigma^\mathrm{P}_{\mathrm{B^{3+}}}}\frac{d\mu^\mathrm{P}_{\mathrm{B_2O_3}}}{dx}\right]\end{aligned} \tag{A.60}$$

In the case of the perovskite phase (P), Eq. (A.14) has to combined with the cation fluxes in Eq. (A.27) to (A.32):

$$\begin{aligned}\frac{1}{V^\mathrm{P}_\mathrm{m}}\frac{\mathrm{d}(\Delta x_\mathrm{P})}{\mathrm{d}t} &= 3j^\mathrm{M}_{\mathrm{A^{3+}}} - 7j^\mathrm{P}_{\mathrm{A^{3+}}} + 4j^\mathrm{G}_{\mathrm{A^{3+}}} = -\left(3j^\mathrm{M}_{\mathrm{B^{3+}}} - 7j^\mathrm{P}_{\mathrm{B^{3+}}} + 4j^\mathrm{G}_{\mathrm{B^{3+}}}\right) \\ &= -\frac{1}{(3F)^2}\left[\frac{9}{2}\frac{\sigma^\mathrm{M}_{\mathrm{A^{3+}}}\sigma^\mathrm{M}_{\mathrm{B^{3+}}}}{\sigma^\mathrm{M}_{\mathrm{A^{3+}}}+\sigma^\mathrm{M}_{\mathrm{B^{3+}}}}\frac{\mathrm{d}\mu^\mathrm{M}_{\mathrm{A_2O_3}}}{\mathrm{dx}} - 7\frac{\sigma^\mathrm{P}_{\mathrm{A^{3+}}}\sigma^\mathrm{P}_{\mathrm{B^{3+}}}}{\sigma^\mathrm{P}_{\mathrm{A^{3+}}}+\sigma^\mathrm{P}_{\mathrm{B^{3+}}}}\frac{\mathrm{d}\mu^\mathrm{P}_{\mathrm{A_2O_3}}}{\mathrm{dx}} + \frac{16}{5}\frac{\sigma^\mathrm{G}_{\mathrm{A^{3+}}}\sigma^\mathrm{G}_{\mathrm{B^{3+}}}}{\sigma^\mathrm{G}_{\mathrm{A^{3+}}}+\sigma^\mathrm{G}_{\mathrm{B^{3+}}}}\frac{d\mu^\mathrm{G}_{\mathrm{A_2O_3}}}{\mathrm{dx}}\right] \\ &= \frac{1}{(3F)^2}\left[\frac{9}{4}\frac{\sigma^\mathrm{M}_{\mathrm{A^{3+}}}\sigma^\mathrm{M}_{\mathrm{B^{3+}}}}{\sigma^\mathrm{M}_{\mathrm{A^{3+}}}+\sigma^\mathrm{M}_{\mathrm{B^{3+}}}}\frac{\mathrm{d}\mu^\mathrm{M}_{\mathrm{B_2O_3}}}{\mathrm{dx}} - 7\frac{\sigma^\mathrm{P}_{\mathrm{A^{3+}}}\sigma^\mathrm{P}_{\mathrm{B^{3+}}}}{\sigma^\mathrm{P}_{\mathrm{A^{3+}}}+\sigma^\mathrm{P}_{\mathrm{B^{3+}}}}\frac{\mathrm{d}\mu^\mathrm{P}_{\mathrm{B_2O_3}}}{\mathrm{dx}} + \frac{16}{3}\frac{\sigma^\mathrm{G}_{\mathrm{A^{3+}}}\sigma^\mathrm{G}_{\mathrm{B^{3+}}}}{\sigma^\mathrm{G}_{\mathrm{A^{3+}}}+\sigma^\mathrm{G}_{\mathrm{B^{3+}}}}\frac{d\mu^\mathrm{G}_{\mathrm{B_2O_3}}}{\mathrm{dx}}\right]\end{aligned} \tag{A.61}$$

The growth rate of the garnet phase (G) in Eq. (A.62) is gained from Eq. (A.15) and the cation fluxes in Eq. (A.29) to (A.32):

$$\begin{aligned}\frac{1}{V^\mathrm{G}_\mathrm{m}}\frac{\mathrm{d}(\Delta x_\mathrm{G})}{\mathrm{d}t} &= j^\mathrm{P}_{\mathrm{A^{3+}}} - \frac{4}{3}j^\mathrm{G}_{\mathrm{A^{3+}}} = -\left(j^\mathrm{P}_{\mathrm{B^{3+}}} - \frac{4}{3}j^\mathrm{G}_{\mathrm{B^{3+}}}\right) \\ &= -\frac{1}{(3F)^2}\left[\frac{\sigma^\mathrm{P}_{\mathrm{A^{3+}}}\sigma^\mathrm{P}_{\mathrm{B^{3+}}}}{\sigma^\mathrm{P}_{\mathrm{A^{3+}}}+\sigma^\mathrm{P}_{\mathrm{B^{3+}}}}\frac{\mathrm{d}\mu^\mathrm{P}_{\mathrm{A_2O_3}}}{\mathrm{d}x} - \frac{16}{15}\frac{\sigma^\mathrm{G}_{\mathrm{A^{3+}}}\sigma^\mathrm{G}_{\mathrm{B^{3+}}}}{\sigma^\mathrm{G}_{\mathrm{A^{3+}}}+\sigma^\mathrm{G}_{\mathrm{B^{3+}}}}\frac{\mathrm{d}\mu^\mathrm{G}_{\mathrm{A_2O_3}}}{\mathrm{d}x}\right] = \frac{1}{(3F)^2}\left[\frac{\sigma^\mathrm{P}_{\mathrm{A^{3+}}}\sigma^\mathrm{P}_{\mathrm{B^{3+}}}}{\sigma^\mathrm{P}_{\mathrm{A^{3+}}}+\sigma^\mathrm{P}_{\mathrm{B^{3+}}}}\frac{\mathrm{d}\mu^\mathrm{P}_{\mathrm{B_2O_3}}}{\mathrm{d}x} - \frac{16}{9}\frac{\sigma^\mathrm{G}_{\mathrm{A^{3+}}}\sigma^\mathrm{G}_{\mathrm{B^{3+}}}}{\sigma^\mathrm{G}_{\mathrm{A^{3+}}}+\sigma^\mathrm{G}_{\mathrm{B^{3+}}}}\frac{\mathrm{d}\mu^\mathrm{G}_{\mathrm{B_2O_3}}}{\mathrm{d}x}\right]\end{aligned} \tag{A.62}$$

If there is no growth of the adjacent phases, the complex expression for the growth rate of a product layer in Eq. (A.60), (A.61) or (A.62) will be reduced to simple parabolic rate equation $d(\Delta x_i)/dt = k_{\mathrm{Tam},\,i}/\Delta x_i$ (i = M, P and G), as the chemical potential gradients of A_2O_3 and B_2O_3 in the adjacent phases are each set to zero:

$$\frac{1}{V^\mathrm{M}_\mathrm{m}}\frac{\mathrm{d}(\Delta x_\mathrm{M})}{\mathrm{d}t} = \frac{9}{4}\frac{1}{(3F)^2}\frac{\sigma^\mathrm{M}_{\mathrm{A^{3+}}}\sigma^\mathrm{M}_{\mathrm{B^{3+}}}}{\sigma^\mathrm{M}_{\mathrm{A^{3+}}}+\sigma^\mathrm{M}_{\mathrm{B^{3+}}}}\frac{\mathrm{d}\mu^\mathrm{M}_{\mathrm{A_2O_3}}}{\mathrm{d}x} \tag{A.63}$$

$$\frac{1}{V^\mathrm{P}_\mathrm{m}}\frac{\mathrm{d}(\Delta x_\mathrm{P})}{\mathrm{d}t} = 7\frac{1}{(3F)^2}\frac{\sigma^\mathrm{P}_{\mathrm{A^{3+}}}\sigma^\mathrm{P}_{\mathrm{B^{3+}}}}{\sigma^\mathrm{P}_{\mathrm{A^{3+}}}+\sigma^\mathrm{P}_{\mathrm{B^{3+}}}}\frac{\mathrm{d}\mu^\mathrm{P}_{\mathrm{A_2O_3}}}{\mathrm{d}x} \tag{A.64}$$

$$\frac{1}{V_{\mathrm{m}}^{\mathrm{G}}}\frac{\mathrm{d}(\Delta x_{\mathrm{G}})}{\mathrm{d}t}=\frac{16}{15}\frac{1}{(3F)^2}\frac{\sigma_{\mathrm{A}^{3+}}^{\mathrm{G}}\sigma_{\mathrm{B}^{3+}}^{\mathrm{G}}}{\sigma_{\mathrm{A}^{3+}}^{\mathrm{G}}+\sigma_{\mathrm{B}^{3+}}^{\mathrm{G}}}\frac{\mathrm{d}\mu_{\mathrm{A_2O_3}}^{\mathrm{G}}}{\mathrm{d}x} \tag{A.65}$$

Thus, the independent and uncoupled growth of the single reaction systems A_2O_3–$A_4B_2O_9$, $A_4B_2O_9$–$A_3B_5O_{12}$ or $A_3B_5O_{12}$–B_2O_3, as given in Eq. (1), (2) and (3) are described by Eq. (A.63) to (A.65). Accordingly, the parabolic rate constants k_{M}, k_{P} and k_{G} for the independent growth of a product layers yields as follows[7]:

$$k_{\mathrm{M}}=-\frac{9}{4}V_{\mathrm{m}}^{\mathrm{M}}\frac{1}{(3F)^2}\frac{\sigma_{\mathrm{A}^{3+}}^{\mathrm{M}}\sigma_{\mathrm{B}^{3+}}^{\mathrm{M}}}{\sigma_{\mathrm{A}^{3+}}^{\mathrm{M}}+\sigma_{\mathrm{B}^{3+}}^{\mathrm{M}}}\Delta_{\mathrm{R}}G_{\mathrm{M}}^{\circ} \tag{A.66}$$

$$k_{\mathrm{P}}=-49V_{\mathrm{m}}^{\mathrm{P}}\frac{1}{(3F)^2}\frac{\sigma_{\mathrm{A}^{3+}}^{\mathrm{P}}\sigma_{\mathrm{B}^{3+}}^{\mathrm{P}}}{\sigma_{\mathrm{A}^{3+}}^{\mathrm{P}}+\sigma_{\mathrm{B}^{3+}}^{\mathrm{P}}}\Delta_{\mathrm{R}}G_{\mathrm{P}}^{\circ} \tag{A.67}$$

$$k_{\mathrm{G}}=-\frac{16}{9}V_{\mathrm{m}}^{\mathrm{G}}\frac{1}{(3F)^2}\frac{\sigma_{\mathrm{A}^{3+}}^{\mathrm{G}}\sigma_{\mathrm{B}^{3+}}^{\mathrm{G}}}{\sigma_{\mathrm{A}^{3+}}^{\mathrm{G}}+\sigma_{\mathrm{B}^{3+}}^{\mathrm{G}}}\Delta_{\mathrm{R}}G_{\mathrm{G}}^{\circ} \tag{A.68}$$

The chemical potential gradients of the components A_2O_3 and B_2O_3 are expressed by the free reaction enthalpies as given in Eq. (A.54) to (A.59). The Eq. (A.60) to (A.62), describing the simultanous growth of all product layers can be rewritten in a simplified and condensed form when considering the chemical potential gradients of the components A_2O_3 and B_2O_3 in Eq. (A.54) to (A.59) and the parabolic rate constants for the independent and uncoupled growth of a product layers in Eq. (A.66) to (A.68):

$$\frac{1}{V_{\mathrm{m}}^{\mathrm{M}}}\frac{\mathrm{d}(\Delta x_{\mathrm{M}})}{\mathrm{d}t}=\frac{k_{\mathrm{M}}}{V_{\mathrm{m}}^{\mathrm{M}}}\frac{1}{\Delta x_{\mathrm{M}}}-\frac{1}{7}\frac{k_{\mathrm{P}}}{V_{\mathrm{m}}^{\mathrm{P}}}\frac{1}{\Delta x_{\mathrm{P}}} \tag{A.69}$$

$$\frac{1}{V_{\mathrm{m}}^{\mathrm{P}}}\frac{\mathrm{d}(\Delta x_{\mathrm{P}})}{\mathrm{d}t}=-2\frac{k_{\mathrm{M}}}{V_{\mathrm{m}}^{\mathrm{M}}}\frac{1}{\Delta x_{\mathrm{M}}}+\frac{k_{\mathrm{P}}}{V_{\mathrm{m}}^{\mathrm{P}}}\frac{1}{\Delta x_{\mathrm{P}}}-3\frac{k_{\mathrm{G}}}{V_{\mathrm{m}}^{\mathrm{G}}}\frac{1}{\Delta x_{\mathrm{G}}} \tag{A.70}$$

$$\frac{1}{V_{\mathrm{m}}^{\mathrm{G}}}\frac{\mathrm{d}(\Delta x_{\mathrm{G}})}{\mathrm{d}t}=-\frac{1}{7}\frac{k_{\mathrm{P}}}{V_{\mathrm{m}}^{\mathrm{P}}}\frac{1}{\Delta x_{\mathrm{P}}}+\frac{k_{\mathrm{G}}}{V_{\mathrm{m}}^{\mathrm{G}}}\frac{1}{\Delta x_{\mathrm{G}}} \tag{A.71}$$

This is a system of non-linear ODEs with constant coefficients. As the functional expressions for the layer thickness Δx_{M}, Δx_{P} and Δx_{G} should only depend on one variabe, *i.e.* the reaction time Δt, the ODE system in Eq. (A.69) to (A.71) can be solved by means of simple parabolic rate laws:

$$\Delta x_{\mathrm{M}}=\sqrt{2k_{\mathrm{M}}^{'}\Delta t} \tag{A.72}$$

$$\Delta x_{\mathrm{P}}=\sqrt{2k_{\mathrm{P}}^{'}\Delta t} \tag{A.73}$$

$$\Delta x_{\mathrm{G}}=\sqrt{2k_{\mathrm{G}}^{'}\Delta t} \tag{A.74}$$

This is reasonable, as the chemical potentials of the starting oxides A_2O_3 und B_2O_3 in each growing product layer are fixed at the interfaces by the chemical equilibria with the neighbouring product phases and so their chemical potential gradients are only dependent on the layer thicknesses, see Eq. (A.54) to (A.59). In the case of a simultaneous growth of the product layers, this should also result in parabolic rate laws $d(\Delta x_i)/dt = k_i^{'}/\Delta x_i$ (i = M, P and G), as is expected for a diffusion-limited process [1,17] Accordingly, the rate constants introduced in Eq. (A.72) to (A.74) are the "practical" parabolic rate constants k_{M}', k_{P}' and k_{G}' for simultaneous growth in a solid state reaction forming multiple product phases. The following relations between the "true" and "practical" parabolic rate constants can be gained by inserting Eq. (A.72) to (A.74) in the ODE system[8]:

$$\frac{k_{\mathrm{M}}}{V_{\mathrm{m}}^{\mathrm{M}}}=2\frac{k_{\mathrm{M}}^{'}}{V_{\mathrm{m}}^{\mathrm{M}}}+\frac{1}{2}\frac{\sqrt{k_{\mathrm{M}}^{'}k_{\mathrm{P}}^{'}}}{V_{\mathrm{m}}^{\mathrm{P}}}+\frac{3}{2}\frac{\sqrt{k_{\mathrm{M}}^{'}k_{\mathrm{G}}^{'}}}{V_{\mathrm{m}}^{\mathrm{G}}} \tag{A.78}$$

$$\frac{k_{\mathrm{P}}}{V_{\mathrm{m}}^{\mathrm{P}}}=7\frac{\sqrt{k_{\mathrm{M}}^{'}k_{\mathrm{P}}^{'}}}{V_{\mathrm{m}}^{\mathrm{M}}}+\frac{7}{2}\frac{k_{\mathrm{P}}^{'}}{V_{\mathrm{m}}^{\mathrm{P}}}+\frac{21}{2}\frac{\sqrt{k_{\mathrm{P}}^{'}k_{\mathrm{G}}^{'}}}{V_{\mathrm{m}}^{\mathrm{G}}} \tag{A.79}$$

---

[7] In fact, the parabolic rate constants are averaged values, as the partial conductivities of the A^{3+} and B^{3+} cations may be composition/stoichiometry dependent.

[8] By inserting the approach in Eq. (!0.72), (A.73) and (A.74 in the ODE system, Eq. (86) to (88), one obtains the following system of algebraic equations:

$$\frac{1}{V_{\mathrm{m}}^{\mathrm{M}}}\sqrt{k_{\mathrm{M}}^{'}}=\frac{1}{V_{\mathrm{m}}^{\mathrm{M}}}\frac{k_{\mathrm{M}}}{\sqrt{k_{\mathrm{M}}^{'}}}-\frac{1}{7}\frac{1}{V_{\mathrm{m}}^{\mathrm{P}}}\frac{k_{\mathrm{P}}}{\sqrt{k_{\mathrm{P}}^{'}}} \tag{A.75}$$

$$\frac{1}{V_{\mathrm{m}}^{\mathrm{P}}}\sqrt{k_{\mathrm{P}}^{'}}=-2\frac{1}{V_{\mathrm{m}}^{\mathrm{M}}}\frac{k_{\mathrm{M}}}{\sqrt{k_{\mathrm{M}}^{'}}}+\frac{1}{V_{\mathrm{m}}^{\mathrm{P}}}\frac{k_{\mathrm{P}}}{\sqrt{k_{\mathrm{P}}^{'}}}-3\frac{1}{V_{\mathrm{m}}^{\mathrm{G}}}\frac{k_{\mathrm{G}}}{\sqrt{k_{\mathrm{G}}^{'}}} \tag{A.76}$$

$$\frac{1}{V_{\mathrm{m}}^{\mathrm{G}}}\sqrt{k_{\mathrm{G}}^{'}}=-\frac{1}{7}\frac{1}{V_{\mathrm{m}}^{\mathrm{P}}}\frac{k_{\mathrm{P}}}{\sqrt{k_{\mathrm{P}}^{'}}}+\frac{1}{V_{\mathrm{m}}^{\mathrm{G}}}\frac{k_{\mathrm{G}}}{\sqrt{k_{\mathrm{G}}^{'}}} \tag{A.77}$$

This equation system is linear with respect to the set of "true" parabolic rate constants k_{M}, k_{P} and k_{G}, but not with respect to the set of "practical" parabolic rate constants k_{M}', k_{P}' and k_{G}'. Thus, it can only be solved for the first set of variables, see Eq. (A.78) to (A.80).

$$\frac{k_{\mathrm{G}}}{V_{\mathrm{m}}^{\mathrm{G}}}=\frac{\sqrt{k_{\mathrm{M}}^{'}k_{\mathrm{G}}^{'}}}{V_{\mathrm{m}}^{\mathrm{M}}}+\frac{1}{2}\frac{\sqrt{k_{\mathrm{P}}^{'}k_{\mathrm{G}}^{'}}}{V_{\mathrm{m}}^{\mathrm{P}}}+\frac{5}{2}\frac{k_{\mathrm{G}}^{'}}{V_{\mathrm{m}}^{\mathrm{G}}} \tag{A.80}$$

If the “true” parabolic rate constant of a distinct product layer is significantely higher compared to the adjacent product layers, the latter can be neglected, see Eq. (A.75) to (A.77). In this case, the “practical” parabolic constant becomes identical to the “true” parabolic rate constant:

$$k_{\mathrm{M}}\gg k_{\mathrm{P}}\ \Rightarrow\ k_{\mathrm{M}}\approx k_{\mathrm{M}}^{'} \tag{A.81}$$

$$k_{\mathrm{P}}\gg k_{\mathrm{M}},k_{\mathrm{G}}\ \Rightarrow\ k_{\mathrm{P}}\approx k_{\mathrm{P}}^{'} \tag{A.82}$$

$$k_{\mathrm{G}}\gg k_{\mathrm{P}}\ \Rightarrow\ k_{\mathrm{G}}\approx k_{\mathrm{G}}^{'} \tag{A.83}$$

References

[1] H. Schmalzried, Solid State Reactions, Weinheim, Verlag Chemie, 1981.

[2] H. Schmalzried, Chemical Kinetics of Solids, Weinheim, VCH-Verlagsgesellschaft, 1995.

[3] C. Wagner, The evaluation of data obtained with diffusion couples of binary single-phase and multiphase systems, Acta Metall. Mater. 17 (2) (1969) 99–107, https://doi.org/10.1016/0001-6160(69)90131-X.

[4] S.J. Schneider, R.S. Roth, J.L. Waring, Solid state reactions involving oxides of trivalent Cations, J. Res. Natl. Bur. Stand. A: Phys. Chem. 65A (4) (1961) 345–374, https://doi.org/10.6028/jres.065A.037.

[5] M.L. Keith, R. Roy, Structural relations among double oxides of trivalent elements, Amer. Min. 39 (1–2) (1954).

[6] A.S. Gandhi, C.G. Levi, Phase selection in precursor-derived yttrium aluminum garnet and related Al_2O_3-Y_2O_3 compositions, J. Mater. Res. 20 (4) (2005) 1017–1025, https://doi.org/10.1557/JMR.2005.0133.

[7] M. Medraj, R. Hammond, M. Parvez, R. Drew, W. Thompson, High temperature neutron diffraction study of the Al_2O_3–Y_2O_3 system, J. Eur. Ceram. Soc. 26 (2006) 3515–3524, https://doi.org/10.1016/j.jeurceramsoc.2005.12.008.

[8] E. Kupp, S. Kochawattana, S. Lee, S. Misture, G. Messing, Particle size effects on yttrium aluminum garnet (YAG) phase formation by solid-state reaction, J. Mater. Res. 29 (19) (2014) 2303–2311, https://doi.org/10.1557/jmr.2014.224.

[9] R. Hariharan, A. Venkatasubramanian, P. Gopalan, Solid-state synthesis and characterization of Ca-substituted $YAlO_3$ as electrolyte for solid oxide fuel cells, J. Solid State Electrochem. 14 (2010) 1657–1666, https://doi.org/10.1007/s10008-010-1008-x.

[10] J.R. Heffelfinger, C.B. Carter, Evolution of Yttrium Aluminum Garnet Films by Solid-State Reaction, MRS Proceedings 317, 1993, https://doi.org/10.1557/proc-317-553.

[11] M.T. Johnson, J.R. Heffelfinder, P.G. Kotula, C.B. Carter, Microscopy of interfaces in model oxide composites, J. Microsc. 185 (2) (1996) 225–232.

[12] S. Arakawa, H. Kadoura, T. Uyama, K. Takatori, Y. Takeda, T. Tani, Formation of preferentially oriented $Y_3Al_5O_{12}$ film on a reactive sapphire substrate: phase and texture transitions from Y_2O_3, J. Eur. Ceram. Soc. 36 (2016) 663–670.

[13] S. Lakiza, O. Fabrichnaya, C. Wang, M. Zinkevich, F. Aldinger, Phase diagram of the ZrO_2/Gd_2O_3/Al_2O_3 system, J. Eur. Ceram. Soc. 26 (2006) 233–246, https://doi.org/10.1016/j.jeurceramsoc.2004.11.011.

[14] U. Kolitsch, H. Seifert, F. Aldinger, Phase relationships in the system Gd_2O_3–Al_2O_3–SiO_2, J. Alloys Compd. 257 (1–2) (1997) 104–114, https://doi.org/10.1016/S0925-8388(96)03121-0.

[15] N. Toropov, Phase Diagram for Ceramists Vol. 2, American Ceramic Society, Westerbille (OH), 1964, p. 96, fig. 2344 (phase diagram of Y_2O_3–Al_2O_3).

[16] R.S. Roth, Phase Equilibria Diagrams: Phase Diagrams for Ceramics vol. XI, The American Ceramic Society, Westville/Ohio USA, 1995, p. 107.

[17] G. Borchardt, Identification of growth mechanisms in solid state reactions forming parallel layers of two phases, J. Cryst. Growth 54 (2) (1981) 365–368, https://doi.org/10.1016/0022-0248(81)90484-X.

[18] C. Schneider, W. Rasband, K. Eliceiri, NIH Image to ImageJ: 25 years of image analysis, Nat. Methods 9 (2012), https://doi.org/10.1038/nmeth.2089.

[19] C. Korte, A. Peters, D. Hesse, N. Zakharov, J. Janek, Ionic conductivity and activation energy for oxygen ion transport in Superlattices – the Semicoherent multilayer system YSZ (ZrO_2 + 9.5 Mol% Y_2O_3)/Y_2O_3, Phys. Chem. Chem. Phys. 10 (2008) 4623–4635, https://doi.org/10.1039/b801675e.

[20] J. Keppner, C. Korte, J. Schubert, W. Zander, M. Ziegner, D. Stolten, XRD Analysis of Strain States in Epitaxial YSZ / RE_2O_3 (RE = Y, Er) Multilayers as a Function of Layer Thickness, Solid State Ionics 273 (2015) 2–7, the E-MRS Conference, Symposium C "Solid State Ionics: Thin Films for Energy and Information Applications". doi:https://doi.org/10.1016/j.ssi.2014.09.012.

[21] J. Philibert, Atom Movements – Diffusion and Mass Transport in Solids, Monographies de Physique, Les Éditions de Physique, 1991.

[22] P. Kotula, C.B.C. Carter, Kinetics of thin-film reactions of nickel oxide with alumina: I, (0001) and 1120 reaction couples, J. Am. Ceram. Soc. 81 (11) (1998) 2869–2876, https://doi.org/10.1111/j.1151-2916.1998.tb02708.x.

[23] P.G. Kotula, C.B. Carter, Kinetics of thin-film reactions of nickel oxide with alumina: II, 1100 and 1102 reaction couples, J. Am. Ceram. Soc. 81 (11) (1998) 2877–2884, https://doi.org/10.1111/j.1151-2916.1998.tb02709.x.

[24] P.G. Kotula, C.B. Carter, Interfacial control of reaction kinetics in oxides, Phys. Rev. Lett. 77 (1996) 3367, https://doi.org/10.1103/PhysRevLett.77.3367.

[25] C. Korte, B. Franz, D. Hesse, Electric field driven solid state reactions – reaction kinetics and the influence of grain boundaries on the interface morphology in the system MgO/$MgIn_2O_4$/In_2O_3, Phys. Chem. Chem. Phys. 7 (2005) 413–420.

[26] H. Schmalzried, T. Pfeiffer, The build-up of internal pressures during compound formation, Z. Phys. Chem. N.F. 148 (1986) 21–32.

[27] C.-M. Liu, J.-C. Chen, C.-J. Chen, The growth of an epitaxial Mg–Al spinel layer on sapphire by solid-state reactions, J. Cryst. Growth 285 (1–2) (2005) 275–283, https://doi.org/10.1016/j.jcrysgro.2005.08.023.

[28] L. Bates, J.E. Gamier, Electrical conductivity of $MgAl_2O_4$ and $Y_3Al_5O_{12}$, J. Am. Ceram. Soc. 64 (10) (1981) C138–C141, https://doi.org/10.1111/j.1151-2916.1981.tb10237.x.

[29] A. Christensen, R. Hazell, A comparison of three sets of diffraction data for $Al_2Y_4O_9$: X-ray synchrotron powder data, X-ray single crystal data from Ag K alpha radiation, and neutron single crystal data from 1.01 Angstroem neutrons, Acta Chem. Scand. 45 (1991) 226–230, https://doi.org/10.3891/acta.chem.scand.45-0226.

[30] W.Y. Ching, Y.N. Xu, Nonscalability and nontransferability in the electronic properties of the Y-Al-O system, Phys. Rev. B 59 (20) (1999) 12815.

[31] L. Vasylechko, A. Matkovskii, D. Savytskii, A. Suchocki, F. Wallrafen, Crystal structure of $GdFeO_3$-type rare earth gallates and aluminates, J. Alloys Compd. 291 (1999) 57–65, https://doi.org/10.1016/S0925-8388(99)00247-9.

[32] Ł. Dobrzycki, E. Bulska, D.A. Pawlak, Z. Frukacz, K. Woźniak, Structure of YAG crystals doped/substituted with erbium and ytterbium, Inorg. Chem. 43 (24) (2004) 7656–7664, https://doi.org/10.1021/ic049920z.

[33] O. Fabrichnaya, H.J. Seifert, T. Ludwig, F. Aldinger, A. Navrotsky, The assessment of thermodynamic parameters in the Al_2O_3-Y_2O_3 system and phase relations in the Y-Al-O system, Scand. J. Metall. 30 (3) (2001) 175–183, https://doi.org/10.1034/j.1600-0692.2001.300308.x.

[34] O. Fabrichnaya, H.J. Seifert, R. Weiland, T. Ludwig, F. Aldinger, A. Navrotsky, Phase equilibria and thermodynamics in the Y_2O_3-Al_2O_3-SiO_2 system, Z. Metallkd. 92 (9) (2001) 1083.